

# AIPcS<sub>4</sub>-PDT for gastric cancer therapy using gold nanorod, cationic liposome, and Pluronic<sup>®</sup> F127 nanomicellar drug carriers

Jing Xin<sup>1,\*</sup>  
Sijia Wang<sup>1,\*</sup>  
Bing Wang<sup>1</sup>  
Jiazhuang Wang<sup>1</sup>  
Jing Wang<sup>1</sup>  
Luwei Zhang<sup>1</sup>  
Bo Xin<sup>2</sup>  
Lijian Shen<sup>1</sup>  
Zhenxi Zhang<sup>1</sup>  
Cuiping Yao<sup>1</sup>

<sup>1</sup>Key Laboratory of Biomedical Information Engineering of Education Ministry, Institute of Biomedical Analytical Technology and Instrumentation, School of Life Science and Technology, Xi'an Jiaotong University, Xi'an, Shaanxi, China; <sup>2</sup>School of Innovation and Entrepreneurship, Xi'an Fan Yi University, Xi'an, Shaanxi, China

\*These authors contributed equally to this work

**Purpose:** As a promising photodynamic therapy (PDT) agent, Al(III) phthalocyanine chloride tetrasulfonic acid (AIPcS<sub>4</sub>) provides deep penetration into tissue, high quantum yields, good photostability, and low photobleaching. However, its low delivery efficiency and high binding affinity to serum albumin cause its low penetration into cancer cells, further limiting its PDT effect on gastric cancer. In order to improve AIPcS<sub>4</sub>/PDT effect, the AIPcS<sub>4</sub> delivery systems with different drug carriers were synthesized and investigated.

**Materials and methods:** Gold nanorods, cationic liposomes, and Pluronic<sup>®</sup> F127 nanomicellars were used to formulate the AIPcS<sub>4</sub> delivery systems. The anticancer effect was evaluated by CCK-8 assay and colony formation assay. The delivery efficiency of AIPcS<sub>4</sub> and the binding affinity to serum proteins were determined by fluorescence intensity assay. The apoptosis and necrosis ability, reactive oxygen species and singlet oxygen generation, mitochondrial transmembrane potential and ([Ca<sup>2+</sup>]<sub>i</sub>) concentration were further measured to evaluate the mechanism of cell death.

**Results:** The series of synthesized AIPcS<sub>4</sub> delivery systems with different drug carriers improve the limited PDT effect in varying degrees. In contrast, AIPcS<sub>4</sub> complex with gold nanorods has significant anticancer effects because gold nanorods are not only suitable for AIPcS<sub>4</sub> delivery, but also exhibit enhanced singlet oxygen generation effect and photothermal effect to induce cell death directly. Moreover, AIPcS<sub>4</sub> complex with cationic liposomes shows the potent inhibition effect because of its optimal AIPcS<sub>4</sub> delivery efficiency and ability to block serum albumin. In addition, AIPcS<sub>4</sub> complex with Pluronic F127 exhibits inferior PDT effect but presents lower cytotoxicity, slower dissociation rate, and longer retention time of incorporated drugs; thus, F127-AIPcS<sub>4</sub> is used for prolonged gastric cancer therapy.

**Conclusion:** The described AIPcS<sub>4</sub> drug delivery systems provide promising agents for gastric cancer therapy.

**Keywords:** drug delivery carriers, AIPcS<sub>4</sub>, gastric cancer therapy, gold nanoparticles, cationic liposome, nanomicelle

## Introduction

Gastric cancer is the third leading cause of cancer-associated death.<sup>1</sup> It exhibits high incidence and mortality and is a major public health issue worldwide. Surgery is the most common gastric cancer treatment strategy, and it allows for the removal of the tumor mass.<sup>2</sup> Chemical and physical treatments significantly hamper the rapid growth of gastric cancer cells, especially during chemotherapy and radiotherapy. Furthermore, surgery combined with neoadjuvant chemotherapy or radiotherapy is used to enhance the therapeutic indices for gastric cancer.<sup>3</sup> However, these treatment strategies inhibit normal cell growth. Severe side effects, high toxicity, and drug resistance usually lead

Correspondence: Zhenxi Zhang;  
Cuiping Yao  
School of Life Sciences and Technology,  
Xi'an Jiaotong University, Number 28  
Xian Ning West Road, Xi'an, Shaanxi  
710049, China  
Tel/fax +86 82 6632 8683  
Email zxzhang@mail.xjtu.edu.cn;  
zsycc@mail.xjtu.edu.cn

to the failure of cancer treatment methods, thereby leading to low quality of life.<sup>4</sup> The prominent antitumor growth treatment response and low toxic side effects of photodynamic therapy (PDT) against various cancers depend on the tumor-selective accumulation of the photosensitizer.<sup>5,6</sup> PDT has been brought into focus for its high efficiency, safety, small operational wound, few side effects, synergy compatibility, repeatability, relatively low cost, etc.<sup>7,8</sup> Under light activation, the photosensitizer generates reactive oxygen species (ROS) to induce oxidative stress, which can damage cellular organelles and membranes, thereby leading to apoptosis or necrosis of the neoplastic tissue.<sup>5,9</sup> Moreover, PDT leads to indirect tumor ablation by causing tumor ischemia and nutritional starvation through vascular leakage, blood flow stasis, and vascular collapse.<sup>10,11</sup> Therefore, PDT is a promising method for gastric cancer therapy.

The photosensitizer is the core of PDT. However, the low delivery efficiency and limited antitumor effect of the photosensitizer, as well as the shallow tissue penetration depth of the light source, remain problematic.<sup>12,13</sup> The development of a new effective photosensitizer or the modification of existing photosensitizers is important to increase PDT effect. Al(III) phthalocyanine chloride tetrasulfonic acid (AIPcS<sub>4</sub>), a derivative of photofrin, is a second-generation photosensitizer. Based on its emission spectra in the near-infrared region (NIR), AIPcS<sub>4</sub> offers deep tissue penetration, high quantum yields, good photostability, low photo bleaching, etc. Thus, AIPcS<sub>4</sub> has been widely used as a photosensitizer for cancer treatments.<sup>14,15</sup> AIPcS<sub>4</sub> exhibits superior PDT effects in various cancer cell lines.<sup>16-22</sup> However, little is known about its ability to inhibit gastric cancer cell growth and proliferation as well as its possible mechanism of cell death (ie, apoptosis or necrosis). In this study, we evaluate the anti-growth effects of AIPcS<sub>4</sub> on gastric cancer cells. Unfortunately, its inhibitory effect is limited. To discover the main reason behind the limited PDT effects and further improve its antitumor ability, the delivery efficiency of AIPcS<sub>4</sub> was investigated by evaluating its fluorescence intensity in gastric cancer cells. The results revealed that AIPcS<sub>4</sub> penetrates poorly into cells. Hence, increasing the delivery efficiency of AIPcS<sub>4</sub> may be an effective way to increase its antitumor effects via PDT. In addition, human serum albumin (HSA) shows high binding affinity to negatively charged molecules, including AIPcS<sub>4</sub>.<sup>23,24</sup> Therefore, preventing the binding of AIPcS<sub>4</sub> to HSA effectively may be a good strategy to increase its ability to penetrate cancer cells and further improve its anticancer effects. Generally, finding effective strategies to increase the delivery efficiency of AIPcS<sub>4</sub> and reduce its binding affinity to HSA will enhance its PDT antitumor effects on gastric cancer therapy.

Using organic and inorganic nanomaterials to formulate an ideal PDT system has been verified as an effective strategy to enhance the delivery efficiency and PDT effect of the photosensitizer.<sup>25</sup> These nanosized carriers mainly include liposomes, natural polymeric nanoparticles (albumin, chitosan, hyaluronic acid, etc), synthetic polymers (polymeric micelle, polymer, homopolymer, hydrogel, etc), quantum dots, ceramic-based nanoparticles, metallic nanoparticles, carbon materials, and so on.<sup>26-38</sup> Among them, a PDT system based on gold nanomaterials significantly increased the delivery efficiency of photosensitizers and enhanced the antitumor effects in various cancer treatments.<sup>39-42</sup> Gold nanoparticles increase the binding affinity and tumor-selective uptake of the photosensitizer because of their nanoscale size and the enhanced permeability and retention effect. In addition, the enhancement of PDT effects using gold nanoparticles can be obtained because of the local electric enhancement and singlet oxygen (SOG) enhancement induced by the localized surface plasmon resonance of gold nanoparticles.<sup>43</sup> Gold nanorods (AuNR), which are positively charged and elongated gold nanoparticles, have attracted considerable attention for their unique properties, including efficient large-scale synthesis, high optical absorption coefficients in the NIR, and precisely tunable light absorption range through aspect ratio adjustment.<sup>36,44</sup> In cancer therapy research, AuNR demonstrate significant antitumor growth ability because of their high photothermal conversion efficiency via NIR laser irradiation. Jang et al has synthesized a multifunctional nanomedicine platform through AuNR conjugated with AIPcS<sub>4</sub> to perform NIR-triggered controllable AIPcS<sub>4</sub> release, increase AIPcS<sub>4</sub> delivery efficiency, and reduce the binding affinity to the serum albumin, ultimately improving squamous cell carcinoma therapy based on the synergy between PDT and photothermal therapy (PTT).<sup>23</sup> Hence, the complex of AuNR–AIPcS<sub>4</sub> may improve the limited AIPcS<sub>4</sub>/PDT effects on gastric cancer. Beyond that, we noticed that the modification method of AuNR described in their research to increase the surface charge using a positively charged peptide, was mainly based on thiol chemical. But the positively charged peptide can also be modified on the polyethylene glycol (PEG) chain through –NH<sub>2</sub> and –COOH interactions. Therefore, the load efficiency of AIPcS<sub>4</sub> may further increase. In this study, we evaluated the synthesized method of AuNR–AIPcS<sub>4</sub> based on polymer and further researched the anti-growth effect on gastric cancer.

With the exception of AuNR, lipid-based drug carriers have been used for photosensitizer delivery because of their low systemic toxicity and long drug circulation time.<sup>26,45</sup> Young et al and Derycke et al synthesized the AIPcS<sub>4</sub>–PDT systems based on liposome and showed that the AIPcS<sub>4</sub>-loaded

liposome enhanced the phototoxicity on HSC-3 cells and exhibited weak PDT therapy effect on Hela cells and AY-27 cells.<sup>17,46</sup> This indicates that the antitumor effect of the PDT system based on liposome was dependent on cell type. Among functionalized liposomes, the cationic liposome (Clip) has attracted more attention due to its high intracellular bioavailability.<sup>47</sup> Clip can be absorbed to the surface of negatively charged cellular membranes via electrostatic attraction. Furthermore, PEG-incorporated Clip can prolong drug circulation time to promote passive tumor targeting ability and increase drug delivery efficiency.<sup>48,49</sup> Little information is available regarding the use of Clip for photosensitizer delivery; however, Clip may be another promising AlPcS<sub>4</sub> delivery vector to improve anticancer effect on gastric cancer by increasing AlPcS<sub>4</sub> delivery efficiency, reducing AlPcS<sub>4</sub> binding affinity to HSA, and enhancing AlPcS<sub>4</sub> intracellular uptake.

Pluronic® block copolymer (also named as poloxamer), another efficient drug delivery vector, has noteworthy applications in drug delivery systems.<sup>50</sup> Pluronic® F127 is one of the most common types and consists of hydrophilic polyethylene oxide (PEO) and lipophilic polypropylene oxide (PPO) blocks, which are arranged in a basic PEO–PPO–PEO structure.<sup>51</sup> In aqueous solutions, Pluronic F127 can self-assemble easily to form nanosize micelles with unique core–shell structures. The micelle core is composed of a PPO block and the hydrated shell is composed of PEO. Compared with other classical surfactant-based drug delivery systems, Pluronic F127 demonstrates higher delivery efficiency and promotes higher drug accumulation to the target site because of its slower rate of dissociation, thus allowing prolonged retention of incorporated drugs.<sup>50</sup> Park and Na revealed that the cellular internalization and tumor-specific targeting efficiency of Chlorin e6 were improved through conjugating to F127.<sup>33,52</sup> However, compared with insoluble photosensitizer, very few studies have been made on the incorporation of hydrophilic AlPcS<sub>4</sub> photosensitizer based on Pluronic micellar drug delivery vector. Its ability to enhance AlPcS<sub>4</sub> delivery efficiency and improve AlPcS<sub>4</sub>-PDT effect should be studied.

In the present study, we synthesized a series of delivery systems of AlPcS<sub>4</sub> photosensitizer, including AuNR, Clip, and Pluronic F127 nanomicellar, to compare and search a suitable AlPcS<sub>4</sub> delivery platform to increase its delivery efficiency, reduce its binding affinity to HSA, increase its intracellular uptake ability, and ultimately improve the limited AlPcS<sub>4</sub>-PDT antitumor effects on gastric cancer cells. AlPcS<sub>4</sub> delivery efficiency and anticancer activities were more or less improved with the help of AuNR, Clip, and Pluronic F127 nanomicellars. Among them, Clip exhibited

optimal AlPcS<sub>4</sub> drug delivery efficiency. AuNR demonstrated relatively inferior AlPcS<sub>4</sub> drug delivery efficiency; however, AuNR–AlPcS<sub>4</sub> still provided significant antitumor growth effect because of the PTT of AuNR. The F127–AlPcS<sub>4</sub> showed slight PDT antitumor effects compared with the other two compounds; however, low dark cytotoxicity persisted after prolonged treatment, indicating that F127–AlPcS<sub>4</sub> may still be a promising agent for gastric cancer therapy and offers significant antitumor effects. Beyond the antitumor effect of AlPcS<sub>4</sub> with the help of drug carriers, revealing the mechanism of cell death induced by AlPcS<sub>4</sub>-PDT is important to further regulate these processes and potentiate the antitumor growth effects. Hence, we further evaluated the ability of AlPcS<sub>4</sub>-PDT to induce apoptosis or necrosis. Our findings suggested that post-modified AlPcS<sub>4</sub>-PDT could effectively inhibit the growth and proliferation of gastric cancer cells through apoptosis, which mainly involves ROS and SOG production, Ca<sup>2+</sup> release, and mitochondrial membrane potential decrease. In summary, AuNR and Clip have the potential to be used as effective AlPcS<sub>4</sub> carriers for improved intracellular uptake and increased anti-growth effect on gastric cancer while maintaining low cytotoxicity, whereas Pluronic F127 nanomicellar vector is suitable for effective delivery of AlPcS<sub>4</sub> to improve intracellular uptake and increase the anti-growth effect on gastric cancer during prolonged treatment.

## Materials and methods

### Cell lines and reagents

Moderately differentiated human gastric cancer cell line SGC-7901 purchased from the Cell Bank of the Academy of Military Medical Science (Beijing, China) and human immortalized fetal gastric epithelial cell line GES-1 obtained from the Beijing Institute of Cancer Research (China)<sup>53–55</sup> were donated by State Key Laboratory of Cancer Biology, the Digestion Department of Xijing Hospital, and the Fourth Military Medical University (China). SGC-7901 and GES-1 cells were cultured in RPMI 1640 medium (HyClone Laboratories Inc., Logan, UT, USA) supplemented with 10% fetal bovine serum (HyClone) and 1% penicillin/streptomycin in a humidified incubator at 37°C with 5% CO<sub>2</sub>. Cetyltrimethylammonium bromide (CTAB), Pluronic F127, and JC-1 mitochondria staining kit were purchased from Sigma. Sodium borohydride, chloroauric acid (HAuCl<sub>4</sub>), silver nitrate, and ascorbic acid were purchased from Aladdin, Cell Counting kit (CCK-8) from Dojindo, the trypan blue, Hoechst 33258/propidium iodide (PI) staining kits, Fluo-3/AM fluorescence probe from Beyotime Company, thiol PEG succinimidyl NHS (SH–PEG–NHS) from a local supplier,

AlPcS<sub>4</sub> from Frontier Scientific, and dipalmitoyl-sn-glycero-3-phosphocholine (DPPC) cholesterol, and PEG2000-1,2-distearoyl-sn-glycero-3-phosphoethanolamine (DSPE) from Avanti Polar Lipids.

## Synthesis of different drug delivery systems of AlPcS<sub>4</sub>

**AuNR–AlPcS<sub>4</sub> complex:** the synthesized method of 810 nm AuNR is shown in Supplementary materials. First, 1 mg arginine-arginine-leucine-alanine-cysteine peptide (RRLAC) was conjugated on a 1 mg SH–PEG–NHS (molecular weight [MW] 5,000 Da) chain based on the succinimide ester with stirring for 1 hour. Afterward, the mixture solution SH–PEG–RRLAC and unreacted RRLAC were added to 1 mL AuNR solution at PEG: Au molar ratios of  $1 \times 10^5$  and stirred overnight at room temperature. After the reaction, the mixture was centrifuged to remove the unconjugated SH–PEG–RRLAC and RRLAC to obtain AuNR–PEG solution. Sequentially, 200  $\mu$ L of the different concentrations of AlPcS<sub>4</sub> aqueous solution (25–600  $\mu$ g/mL) was added to 1 mL AuNR–PEG solution, and the mixture was stirred overnight at room temperature and away from light. To remove the free AlPcS<sub>4</sub> of the charged complex, the above mixture was passed through a PD-10 desalting column (GE Healthcare). A purified AuNR–AlPcS<sub>4</sub> charged complex was finally obtained and stored at 4°C.

**AlPcS<sub>4</sub>-loaded Clip complex (Clip–AlPcS<sub>4</sub>):** Clip was prepared by the standard thin-film hydration method, followed by polycarbonate membrane extrusion. Briefly, the DPPC, DOTAP, cholesterol, and PEG2000–DSPE were dissolved in chloroform and transferred into a suitable round bottle flask at a ratio of 12:1:3:2. The lipid film was formed by evaporating the chloroform from a round bottle flask under nitrogen stream. Residual chloroform was removed, and the lipid film was then dried in a desiccator under vacuum overnight. Afterward, 500  $\mu$ L of AlPcS<sub>4</sub> solution (250  $\mu$ g/mL) was added into the vessel containing the lipid film at 48°C, which was greater than the highest fluid–solid transition temperature (T<sub>m</sub>: 45°C) of the lipids in the mixture. After 20 minutes of incubation, the mixture was gently stirred, transferred to an ice bath, and incubated again for 12 minutes. After incubation, the vessel was transferred to a 48°C water bath and incubated again for 12 minutes, stirred gently, transferred to an ice bath, and incubated again for 12 minutes. These steps were repeated six times. The multilamellar vesicle suspension loaded with AlPcS<sub>4</sub> was then passed through a 100-nm polycarbonate membrane 13 times by using a mini-extruder system (Avanti Polar Lipids, Alabaster, AL, USA) to form unilamellar vesicles loaded with AlPcS<sub>4</sub>. Afterward, the

unencapsulated AlPcS<sub>4</sub> was removed by a PD-10 Sephadex column (GE Healthcare). A purified CliP–AlPcS<sub>4</sub> complex was obtained finally and was stored at 4°C.

**Pluronic F127 incorporated AlPcS<sub>4</sub> complex (F127–AlPcS<sub>4</sub>):** 10 milligrams of Pluronic F127 was dissolved in absolute ethyl alcohol solution and stirred until the solution became clear. Afterward, 2.5 mg AlPcS<sub>4</sub> was dissolved in PBS and stirred until dissolved completely. F127 ethyl alcohol solution was added dropwise in the AlPcS<sub>4</sub> PBS solution, and the mixture solution was stirred overnight in the dark. To remove the free AlPcS<sub>4</sub> and absolute ethyl alcohol solution, dialysis was performed in PBS solution for 1 day. Then, the obtained solution was lyophilized to obtain the final purified product, F127–AlPcS<sub>4</sub>.

## Characterization of different drug carriers of AlPcS<sub>4</sub>

The morphologies of AuNR–AlPcS<sub>4</sub>, Clip–AlPcS<sub>4</sub>, and F127–AlPcS<sub>4</sub> were observed using transmission electron microscopy (TEM; JEM-2100, JEOL, Tokyo, Japan). Dynamic light scattering (DLS) of Clip, Clip–AlPcS<sub>4</sub>, F127, and F127–AlPcS<sub>4</sub> were measured using a Malvern Zetasizer Nano ZS (ZS90, Malvern Instruments Ltd, Malvern, UK). The fluorescence spectra (including fluorescence excitation spectra and fluorescence emission spectra) of AuNR–AlPcS<sub>4</sub> with or without 808 nm laser irradiation, Clip–AlPcS<sub>4</sub>, F127–AlPcS<sub>4</sub>, and free AlPcS<sub>4</sub> were measured by a fluorescence spectrophotometer (F-4500, HITACHI, Tokyo, Japan). Zeta potentials of AuNR, AuNR–AlPcS<sub>4</sub>, Clip, Clip–AlPcS<sub>4</sub>, F127, and F127–AlPcS<sub>4</sub> were observed using the same Malvern Zetasizer Nano ZS. Absorption spectra and stability of AuNR–AlPcS<sub>4</sub>, Clip–AlPcS<sub>4</sub>, and F127–AlPcS<sub>4</sub> were recorded using an ultraviolet–visible spectrophotometer (V-550 UV/VIS, JASCO, Tokyo, Japan).

## Cell viability assay

Cell viability assay was used to evaluate the dark cytotoxicity, and the anti-growth effects of AuNR–AlPcS<sub>4</sub>, CliP–AlPcS<sub>4</sub>, and F127–AlPcS<sub>4</sub> on gastric cancer cells were measured by CCK-8 assay. The cell viabilities induced by AuNR, Clip, and F127 drug carriers themselves were also evaluated. Briefly,  $1 \times 10^4$  SGC-7901 cells were seeded to sterile 96-well flat-bottomed plates and incubated overnight. The diluted AuNR–AlPcS<sub>4</sub>, Clip–AlPcS<sub>4</sub>, and F127–AlPcS<sub>4</sub> solutions or AuNR, Clip, and F127 solutions were added to each well. The AlPcS<sub>4</sub> concentration in the complex was from 0.5 to 8  $\mu$ g/mL. The corresponding concentrations of AuNR, Clip, and F127 were 1.86–3 nM, 9.4–300  $\mu$ g/mL, and 0.94–30  $\mu$ g/mL, respectively. In these plates, three wells containing only cells were used

as controls, and three wells containing only complete culture media were used as blank controls. The posttreated cells were then incubated for 6 hours. After the incubation, the media containing AuNR–AlPcS<sub>4</sub>, Clip–AlPcS<sub>4</sub>, and F127–AlPcS<sub>4</sub> or AuNR, Clip, and F127 were replaced by fresh RPMI 1640 complete culture medium. Cell incubation was continued for 24 hours. After the incubation, the solution containing 100  $\mu$ L RPMI 1640 medium and 10  $\mu$ L CCK-8 reagents was added to each well. The plates were incubated for 1 hour at 37°C again. Finally, the absorbance levels of the plates were measured at 450 nm using a microplate reader (Infinite M200 Pro.; Tecan, Männedorf, Switzerland). Dark cytotoxicity of AuNR–AlPcS<sub>4</sub>, Clip–AlPcS<sub>4</sub>, and F127–AlPcS<sub>4</sub> or AuNR, Clip, and F127 with different concentrations was calculated as  $[(\text{OD of drug treated} - \text{OD of blank control}) / (\text{OD of control} - \text{OD of blank control})] \times 100\%$ . The cytotoxic activity of AuNR–AlPcS<sub>4</sub>, Clip–AlPcS<sub>4</sub>, and F127–AlPcS<sub>4</sub> on GES-1 cells was also evaluated.

Similar to the dark cytotoxicity assay, cells were treated in the same manner described previously to evaluate the anti-growth effects. Different from the dark cytotoxicity assay, after replacing the medium containing AuNR–AlPcS<sub>4</sub>, Clip–AlPcS<sub>4</sub>, and F127–AlPcS<sub>4</sub> or AuNR, Clip, and F127 with fresh 1,640 complete culture medium, the cells pretreated with AuNR–AlPcS<sub>4</sub> or AuNR were irradiated with an 808 nm continuous wave laser system for 5 minutes at 100 mW/cm<sup>2</sup> radiant exposure and then irradiated with a 635 nm continuous wave laser system for 3 minutes with 100 mW/cm<sup>2</sup> radiant exposure. The cells pretreated with Clip–AlPcS<sub>4</sub> or F127–AlPcS<sub>4</sub> were irradiated by a 635 nm continuous wave laser system for 5 minutes with 100 mW/cm<sup>2</sup> radiant exposure. Then, the cells were incubated at 37°C with 5% CO<sub>2</sub> for 24 hours. Anti-growth effect analysis using CCK-8 was then repeated.

## Colony formation assay by crystal violet staining

With the exception of anti-growth ability, the antiproliferation effect is also an important evaluation indicator for PDT therapy. To assess antiproliferation effects of AuNR–AlPcS<sub>4</sub>, Clip–AlPcS<sub>4</sub>, F127–AlPcS<sub>4</sub>, and AlPcS<sub>4</sub> and compare their differences, the colony formation assay was done by crystal violet staining. Briefly,  $1 \times 10^3$  cells of SGC-7901 were seeded into each well of the sterile 24-well flat-bottomed plates and incubated overnight. The cells were then treated with AuNR–AlPcS<sub>4</sub>, Clip–AlPcS<sub>4</sub>, F127–AlPcS<sub>4</sub>, or free AlPcS<sub>4</sub> from 0.5  $\mu$ g/mL to 8  $\mu$ g/mL for 6 hours. After incubation, the cells were washed twice with PBS, replaced with fresh complete medium, irradiated by the corresponding laser system, and incubated again for 12 days. During incubation, the medium

was changed every 2 days. After treatment, the cells were washed with PBS twice, fixed with 4% paraformaldehyde fixative for 10 minutes, stained with crystal violet for 5 minutes, washed again, and photographed. Adobe Photoshop was used to quantify the results. Considering that one treatment effect may not be maintained for a long time, the antiproliferation effect in repeated therapy was also evaluated. After seeding in sterile 24-well plates and adhering securely, the cells were treated in the same way described earlier every 3 days for a total of 12 days. After the incubation, the corresponding irradiation was done. Lastly, the colony formation results were imaged and quantified again.

## Fluorescence intensity assay and fluorescence imaging of different drug carriers of AlPcS<sub>4</sub>

To estimate the delivery efficiency and compare the differences of AlPcS<sub>4</sub> for the pre- and post-modifications of drug delivery vectors, the fluorescence intensity assay was done by using a fluorescence spectrophotometer, and fluorescence imaging was recorded with a Nikon eclipse Ti fluorescence microscope (Nikon, Tokyo, Japan). Briefly,  $2.5 \times 10^5$  SGC-7901 cells were seeded into six-well plates and allowed to attach overnight. Then, the cells were treated with different concentrations of AuNR–AlPcS<sub>4</sub>, Clip–AlPcS<sub>4</sub>, F127–AlPcS<sub>4</sub>, or free AlPcS<sub>4</sub> and incubated for 6 hours at 37°C with 5% CO<sub>2</sub>. After the incubation, the cells were washed twice with PBS, digested with trypsin enzyme, collected by centrifugation, and then the emission spectrum was measured at 635 nm excitation wavelength. For fluorescence imaging, the posttreated cells were washed with PBS and imaged. Based on the self-quenching feature of AlPcS<sub>4</sub> at the surface of AuNR, the fluorescence intensity and fluorescence imaging of AuNR–AlPcS<sub>4</sub> after being irradiated by 808 nm continuous wave laser system were further evaluated.

## Inhibition effect on the AlPcS<sub>4</sub> binding affinity to serum proteins for the different drug carriers of AlPcS<sub>4</sub>

To evaluate the inhibition effect of the AlPcS<sub>4</sub> binding affinity to the serum proteins with the help of different drug delivery vectors, the inhibition rates of the fluorescence intensities of AuNR–AlPcS<sub>4</sub>, Clip–AlPcS<sub>4</sub>, F127–AlPcS<sub>4</sub>, and AlPcS<sub>4</sub> in the presence of different serum concentrations were detected using a fluorescence spectrophotometer. AuNR–AlPcS<sub>4</sub>, Clip–AlPcS<sub>4</sub>, F127–AlPcS<sub>4</sub>, and AlPcS<sub>4</sub> were diluted using PBS, PBS containing 10% fetal bovine serum (FBS), and PBS containing 20% FBS to the same concentrations used above, respectively. Fluorescence intensity was then detected using

the fluorescence spectrophotometer under the excitation of 635 nm light. The inhibition rate of fluorescence intensity was calculated as  $(1 - \frac{\text{the fluorescence intensity containing FBS}}{\text{the fluorescence intensity no-containing FBS}}) \times 100\%$ .

### Detection of cell apoptosis and necrosis by Hoechst 33258/PI staining assay

To evaluate whether AuNR–AlPcS<sub>4</sub>, Clip–AlPcS<sub>4</sub>, or F127–AlPcS<sub>4</sub> induced apoptosis or necrosis to inhibit SGC-7901 cell growth, Hoechst 33258/PI staining assay using fluorescence microscopy and flow cytometry was performed according to the manufacturer's instructions. Briefly,  $2.5 \times 10^5$  cells/mL SGC-7901 cells were seeded on bioclean cover slips in six-well plates and allowed to attach overnight. Then, the cells were treated with different concentrations of AuNR–AlPcS<sub>4</sub>, Clip–AlPcS<sub>4</sub>, F127–AlPcS<sub>4</sub>, free AlPcS<sub>4</sub>, and fresh complete culture medium at 37°C with 5% CO<sub>2</sub> for 6 hours. After incubation, the samples were washed twice with PBS, then fresh RPMI 1640 culture medium was added, then they were irradiated with the corresponding laser system, and incubated at 37°C with 5% CO<sub>2</sub> for 24 hours again. After treatment, the cells were stained with Hoechst 33258 and PI dyes for 10 minutes, taken out with cover slips, washed with PBS, mounted on slides with glycerol, and imaged with a fluorescence microscope. To quantify the percentage of apoptosis or necrosis, we counted the number of cells with apoptotic or necrotic characteristics among 200 cells at the high-power field in accordance with the results of stained cell nucleus. In the flow cytometry assay, 2 and 8 µg/mL AlPcS<sub>4</sub> in AuNR–AlPcS<sub>4</sub>, Clip–AlPcS<sub>4</sub>, F127–AlPcS<sub>4</sub>, and free AlPcS<sub>4</sub>, or fresh complete culture medium were added to the cells at 37°C with 5% CO<sub>2</sub> for 6 hours. After completing incubation, the cells were incubated for a further 24 hours with fresh complete culture medium and then harvested, centrifuged at 800 rpm for 5 minutes, washed with PBS, and then stained with Annexin-V FITC for 1 hour and PI for 30 minutes, then analyzed with a FACScan system in the end.

### Measurement of intracellular ROS and SOG generation

ROS and SOG are important factors to induce cell death in PDT. Hence, ROS and SOG concentrations in SGC-7901 cells after being treated with different drug delivery systems of AlPcS<sub>4</sub> or free AlPcS<sub>4</sub> were measured by a 2',7'-Dichlorodihydrofluorescein diacetate (DCFH-DA) fluorescence probe (Beyotime) and singlet oxygen sensor green reagent (SOSGR). SGC-7901 cells were seeded on six-well plates and incubated to adhere securely, then treated

with AuNR–AlPcS<sub>4</sub>, Clip–AlPcS<sub>4</sub>, F127–AlPcS<sub>4</sub>, and free AlPcS<sub>4</sub> at 0.5, 1, 2, 4, and 8 µg/mL for 6 hours. Then, the cells were washed twice with PBS and irradiated with laser systems. For the detection of ROS, cells were harvested and incubated with 10 µmol/L DCFH-DA for 20 minutes at 37°C in complete darkness, washed twice with PBS again, and measured by a fluorescence spectrophotometer under the excitation of 488 nm light. For the detection of SOSGR, the cells were harvested, permeabilized with 0.5% Triton X-100 in PBS for 10 minutes, centrifuged, washed with PBS, mixed with SOSGR, irradiated with 635 nm laser system for 5 minutes, and detected by a fluorescence spectrophotometer under excitation of 504 nm light.

### Determination of mitochondrial transmembrane potential ( $\Delta\Psi_m$ )

Changes in  $\Delta\Psi_m$  of SGC-7901 cells treated with different drug delivery systems of AlPcS<sub>4</sub> and free AlPcS<sub>4</sub> were detected by using a JC-1 mitochondria staining kit according to the manufacturer's instructions. Briefly, the cells were seeded in six-well plates containing bioclean cover slips at  $2.5 \times 10^5$  cells/mL and allowed to attach overnight. Then, the sample was contained in 8 µg/mL AlPcS<sub>4</sub> of AuNR–AlPcS<sub>4</sub>, Clip–AlPcS<sub>4</sub>, F127–AlPcS<sub>4</sub>, free AlPcS<sub>4</sub>, and fresh complete culture medium as control to treat the cells for 6 hours. After treatment, cells were washed twice with PBS, replaced with fresh RPMI 1640 culture medium, stained with JC-1 dye, incubated for 20 minutes, washed with JC-1 assay buffer twice, and imaged by a fluorescent microscope. The mitochondrial depolarization was quantified using ImageJ imaging software. Afterward, changes in  $\Delta\Psi_m$  of SGC-7901 cells after laser light irradiation for 0 and 16 hours were examined, and the method was performed as mentioned earlier.

### Measurement of intracellular calcium ion ([Ca<sup>2+</sup>]<sub>i</sub>) concentration

(Ca<sup>2+</sup>)<sub>i</sub> concentrations of SGC-7901 cells treated with different drug carriers of AlPcS<sub>4</sub> and free AlPcS<sub>4</sub> were measured by using a Fluo-4/AM fluorescence probe. The analysis process involved pretreatment with 8 µg/mL AlPcS<sub>4</sub> of AuNR–AlPcS<sub>4</sub>, Clip–AlPcS<sub>4</sub>, F127–AlPcS<sub>4</sub>, free AlPcS<sub>4</sub>, or free complete culture medium; afterward, SGC-7901 cells were harvested, washed twice with PBS, and incubated with 20M µM Fluo-4/AM for 60 minutes at 37°C in complete darkness. The cells were then washed with PBS and incubated at 37°C for 20 minutes again and then detected by a fluorescence spectrophotometer. The process of fluorescence imaging involved the cells being seeded in six-well plates containing bioclean cover slips at  $2.5 \times 10^5$  cells/mL,

and allowed to attach overnight. The AlPcS<sub>4</sub> drug complexes or free AlPcS<sub>4</sub> were applied to cells for 6 hours at the same concentration as before. After the treatment, the cells were washed twice with PBS and stained with 20 μM Fluo-4/AM dyes for 60 minutes at 37°C in complete darkness and washed with PBS again. After taking out the cover slips, they were mounted on slides with glycerol and imaged with the fluorescence microscope.

## Results and discussion

### Synthesis and characterization of different drug carriers of AlPcS<sub>4</sub>

To increase the delivery efficiency of AlPcS<sub>4</sub> and resolve its poor penetration into gastric cancer cells, the various AlPcS<sub>4</sub> delivery carriers based on AuNR, Clip, and Pluronic F127 were synthesized. First, the TEM of the CTAB-coated 810 nm AuNR showed that its average length and width were 38.35±3.58 and 9.09±1.23 nm, respectively, and its morphology was cylindrical (Figure 1A1). Thiol-terminated monomethoxy poly (ethylene glycol) (mPEG-SH) and RRLAC, which are positively charged short peptides, were sequentially conjugated on the surface of AuNR through thiol chemistry and are responsible for increasing the stability of AuNR and AlPcS<sub>4</sub> loading efficiency of the synthesized AuNR-AlPcS<sub>4</sub>.<sup>23</sup> However, regarding the chemical structure of RRLAC, we found that it conjugates not only on the PEG chain through -NH<sub>2</sub> and -COOH interactions but also on the AuNR surface through -Au and -SH interactions. Then, the PEG chain containing RRLAC can be conjugated to the AuNR surface by thiol chemistry (Figure S1A). Therefore, SH-PEG-NHS is speculated to increase RRLAC loading efficiency to further increase the loading efficiency of AlPcS<sub>4</sub>, compared with mPEG-NHS (Figure S1B). Hence, in this study, HS-PEG-NHS was substituted onto mPEG-SH for modifying AuNR. Results showed that when modified with HS-PEG-NHS and RRLAC, AuNR is displayed as a longitudinal band with a slight red shift to 820 nm (Figure 1A2) and has a high surface zeta potential and stability (Figure S2). Afterward, AlPcS<sub>4</sub> was conjugated onto AuNR-PEG-RRLAC by a charge-charge interaction. When the conjugation was finished, the AuNR longitudinal band remained unchanged, and the maximum AlPcS<sub>4</sub> absorption peak at 675 nm appeared in the new complex (Figure 1A2). Compared with AlPcS<sub>4</sub>, the fluorescence excitation spectrum had a slight change, especially in the range of 600–650 nm, and the maximum excitation peak at about 680 nm had a tiny blue shift. The fluorescence emission spectrum also had a slight change. Before 808 nm laser irradiation, it had about 10 nm blue shift. After 808 nm laser irradiation, it returned

to the AlPcS<sub>4</sub> original position (Figure 1A3). Beyond that, the fluorescence of AlPcS<sub>4</sub> in AuNR-AlPcS<sub>4</sub> complex was quenched. This is caused by the adherence of AlPcS<sub>4</sub> to the AuNR surface inducing the electrons' energy transfer from the AlPcS<sub>4</sub> photosensitizer into AuNR. After 808 nm laser irradiation, AlPcS<sub>4</sub> was released from the AuNR surface, the electrons' energy transfer behavior disappeared, and the fluorescence recovered (Figure S3A).<sup>56</sup> The zeta potential changed from positive to negative (+33 to -10.38 mV; Figure 1A4). The loading efficiency and stability of AlPcS<sub>4</sub> in the HS-PEG-NHS modified method were superior to those of mPEG-SH (Figure S2). In summary, the AuNR-based AlPcS<sub>4</sub> delivery system with SH-PEG-NHS was successfully synthesized; moreover, the synthetic method is more simple and effective. According to the standard curve of AlPcS<sub>4</sub> maximum absorption value and concentration, the encapsulated efficiency of AlPcS<sub>4</sub> in AuNR-AlPcS<sub>4</sub> was approximately 45%.

Gijssens et al and collaborators designed and synthesized a liposome-based AlPcS<sub>4</sub> delivery system to treat cancer, but the results showed that AlPcS<sub>4</sub> slightly accumulated in cells and the weak photocytotoxicity induces limited PDT effects.<sup>19</sup> Compared with other liposomes, Clip possesses some unique advantages as previously described and may be a better fit for AlPcS<sub>4</sub> delivery. Hence, another Clip-based AlPcS<sub>4</sub> drug delivery complex was also synthesized in this study. Figure 1B1 shows the morphology of Clip. Clip-AlPcS<sub>4</sub> has a spherical structure with a lipid bilayer with a relatively nondispersed size of approximately 150 nm, as shown by TEM. Moreover, a finely disseminated pattern occurred. The hydrodynamic size of Clip evaluated by DLS was about 158 nm. The narrow distribution is shown in Figure S4A. The 675 nm maximum absorption peak of AlPcS<sub>4</sub> appeared in the Clip-AlPcS<sub>4</sub> absorption spectrum (Figure 1B2). Compared with AlPcS<sub>4</sub>, its fluorescence excitation spectrum also had a slight change especially in the range of 600–650 nm, and the maximum excitation peak at about 680 nm had about 4 nm blue shift (Figure 1B3). Its fluorescence emission spectrum also had about 3 nm red shift, but the shape of the emission spectrum remained unchanged. In addition, some of the fluorescence of AlPcS<sub>4</sub> in Clip-AlPcS<sub>4</sub> complex was also quenched. This is caused by intraliposomal self-quenching of the fluorescence probe based on concentration-dependent molecular interaction (Figure S3B).<sup>57</sup> In further work, the self-quenching phenomenon can be prevented through optimizing the lipid:photosensitizer ratio. The zeta potential of Clip was 34.5 mV and that of Clip-AlPcS<sub>4</sub> complex was decreased to 8 mV, indicating that AlPcS<sub>4</sub> was predominately included inside the Clip (Figure 1B4). On the basis of the

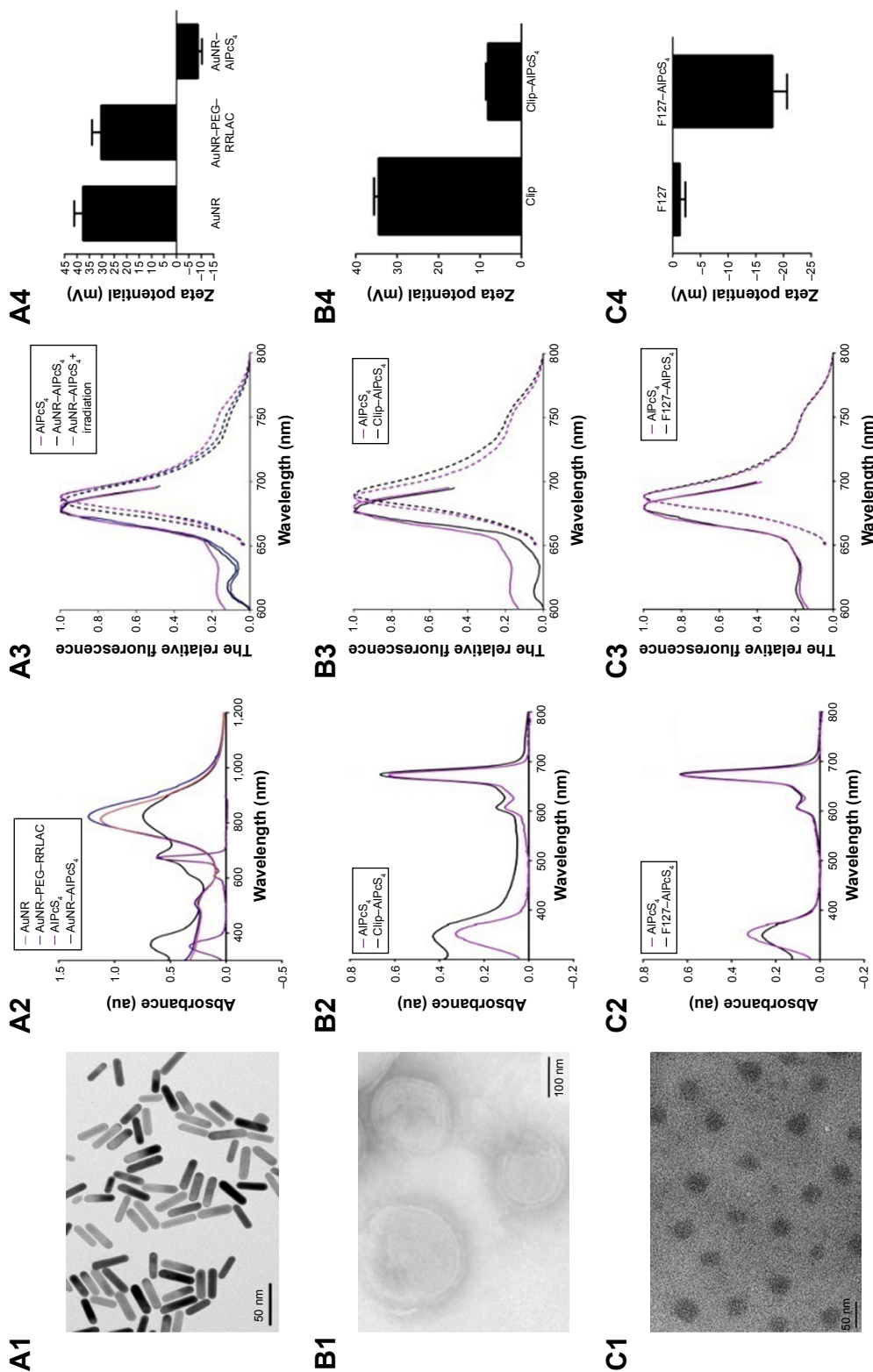


**Figure 1** Synthesis and properties of AlPc<sub>4</sub> delivery complex.

**Notes:** (A1, B1, and C1) Transmission electron microscopy images of AuNR, Clip, and F127; (A2, B2, and C2) UV-vis absorption spectra of compounds in each reactive system; (A3, B3, and C3) Fluorescence spectra (include fluorescence emission spectra [—] and fluorescence excitation spectra [---]) of AuNR-AlPc<sub>4</sub> with or without 808 nm laser irradiation, Clip-AlPc<sub>4</sub>, F127-AlPc<sub>4</sub>, and AlPc<sub>4</sub>; (A4, B4, and C4) Zeta potential of compounds in each reactive system.

**Abbreviations:** AlPc<sub>4</sub>, Al(III) phthalocyanine chloride tetrasulfonic acid; Clip, cationic liposome; RRLAC, arginine-arginine-leucine-alanine-cysteine peptide.

established standard curve, the encapsulated efficiency of AlPcS<sub>4</sub> in Clip–AlPcS<sub>4</sub> reached about 83%.

Beyond modifying existing delivery methods, developing a novel AlPcS<sub>4</sub> delivery approach is important to facilitate the clinical application of AlPcS<sub>4</sub>-PDT. Thus, Pluronic F127 nanomicelle-based AlPcS<sub>4</sub> carriers were designed and synthesized. TEM results showed that F127–AlPcS<sub>4</sub> was 27.6 nm spherical micelles with a finely disseminated pattern (Figure 1C1). The DLS results showed that F127 had a hydrodynamic size of 51 nm and a narrow distribution (Figure S4B). As shown in Figure 1C2, the new maximum absorption peak was consistent with that of AlPcS<sub>4</sub>. Compared with AlPcS<sub>4</sub>, its fluorescence excitation spectrum and fluorescence emission spectrum had no change (Figure 1C3). Only a small amount of fluorescence of AlPcS<sub>4</sub> in F127–AlPcS<sub>4</sub> complex was quenched (Figure S3C). The reason may be similar to Clip–AlPcS<sub>4</sub>. The degree of self-quenching of F127–AlPcS<sub>4</sub> was lower than Clip–AlPcS<sub>4</sub> due to its lower encapsulated efficiency. The zeta potential of F127 was decreased upon coating AlPcS<sub>4</sub>, indicating that F127 coated AlPcS<sub>4</sub> successfully (Figure 1C4). The encapsulated efficiency of AlPcS<sub>4</sub> in F127–AlPcS<sub>4</sub> reached about 40%.

Overall, F127 nanomicelle vector demonstrated the most simple and rapid synthetic method for AlPcS<sub>4</sub> delivery; Clip vector showed the highest encapsulating efficiency, and AuNR and F127 exhibited optimal AlPcS<sub>4</sub> photostability.

## Cytotoxicity and anti-growth effect assay of different drug delivery systems of AlPcS<sub>4</sub>

To evaluate the dark cytotoxicity and anti-growth effects of AuNR–AlPcS<sub>4</sub>, Clip–AlPcS<sub>4</sub>, and F127–AlPcS<sub>4</sub> and the contribution by AuNR, Clip, and F127 carriers themselves on SGC-7901 gastric cancer cells with or without laser irradiation, CCK-8 cell viability analysis was performed. As shown in Figure 2A–C, the cell viability of AuNR–AlPcS<sub>4</sub> slightly decreased as the incorporated AlPcS<sub>4</sub> concentration increased. However, at low concentration, the cell viability still exceeded 80%, and the corresponding AuNR–PEG–RRLAC carriers themselves only induced the inhibition activities was <10% (Figure S5A). Compared with the AuNR–AlPcS<sub>4</sub>, the cell viability of SGC-7901 after being treated with Clip–AlPcS<sub>4</sub> or F127–AlPcS<sub>4</sub> exceeded 90% even at the maximum tested concentration (Figure 2B and C). The Clip and F127 also have less influence on cell viability (Figure S5B and C). Beyond that, the AuNR–AlPcS<sub>4</sub>, Clip–AlPcS<sub>4</sub>, and F127–AlPcS<sub>4</sub> also inhibited the cytotoxic

activity on normal gastric epithelial cells slightly. At the highest concentration, the cell viability still maintained at 87%, 86.5%, and 94%, respectively (Figure S5). Hence, the synthesized AlPcS<sub>4</sub> delivery systems generally exhibited low cytotoxic side effects.

Low cytotoxicity is a stringent requirement for the application of the drug delivery vector, but the significant therapeutic effect is a more important requirement. Hence, cell viability was further evaluated after laser light irradiation, because fluorescence emission and SOG generation of the photosensitizer may be influenced by the distance between gold nanomaterials and photosensitizers. The cells pretreated with AuNR–AlPcS<sub>4</sub> were first irradiated by an 808 nm laser to release AlPcS<sub>4</sub> from the surface of AuNR via AuNR photothermal effects. In the present study, we chose 5 minutes as the irradiation time because 80% fluorescence can be recovered under this condition (Figure S6). Afterward, the cells were exposed to a 635-nm laser to activate ROS and SOG generation of AlPcS<sub>4</sub>, which triggered oxidative stress and effectively damaged the cells. As shown in Figure 2A–C, the cell viability after being treated with AuNR–AlPcS<sub>4</sub> and irradiated by 808 and 635 nm laser light was significantly decreased in a dose-dependent manner. At AlPcS<sub>4</sub> 4 μg/mL concentration, the cell survival rate decreased to about 30%. The cell survival was effectively inhibited while no obvious dark cytotoxicity was exhibited. The PTT effect of AuNR can be used not only for photosensitizer releasing but also for the cancer therapy.<sup>43,58,59</sup> Therefore, the cell viability after being treated with post-modified AuNR and irradiated by 808 nm laser light or by 808 and 635 nm laser lights was evaluated. The results showed that AuNR corresponding to 4 μg/mL and 8 μg/mL AuNR–AlPcS<sub>4</sub> inhibited the growth of cells by about 30% and 50%, respectively. But with further irradiation with 635 nm laser light, the cell viability only slightly decreased. This revealed that AuNR has a significant photothermal effect to induce the cell death upon 808 nm laser light irradiation (Figure S5A). Unlike the AuNR–AlPcS<sub>4</sub> complex, Clip–AlPcS<sub>4</sub> and F127–AlPcS<sub>4</sub> did not require additional stimulation to induce the release of AlPcS<sub>4</sub> from the complex. Hence, the anti-growth effects of Clip–AlPcS<sub>4</sub> and F127–AlPcS<sub>4</sub> were demonstrated after irradiation with 635 nm laser light only, as shown in Figure 2B and C, respectively. Evidently, Clip–AlPcS<sub>4</sub> possessed significant antitumor effect on SGC-7901 cells. At 0.25 μg/mL AlPcS<sub>4</sub> incorporated in Clip–AlPcS<sub>4</sub>, the cell viability was about 80%. As the incorporated AlPcS<sub>4</sub> concentration increased, the cell survival rate significantly decreased in a dose-dependent manner. At 8 μg/mL AlPcS<sub>4</sub>

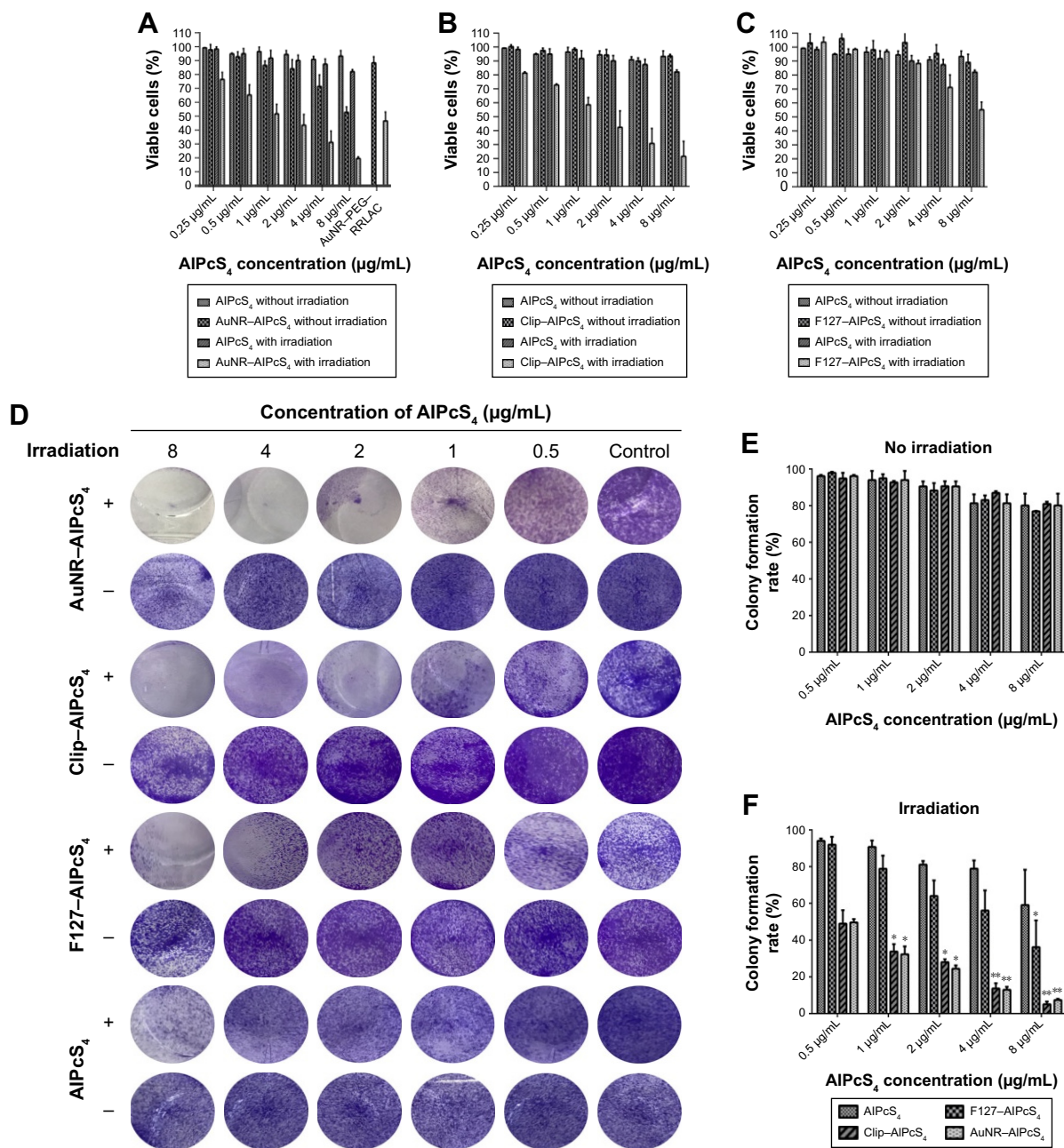


**Figure 2** The anti-growth and antiproliferation effects of AuNR-AIPcS<sub>4</sub>, Clip-AIPcS<sub>4</sub>, and F127-AIPcS<sub>4</sub> on SGC-7901 cells evaluated by the CCK-8 assay and colony formation assay.

**Notes:** (A–C) The dark cytotoxicity (without irradiation) and photocytotoxicity (with irradiation) of AuNR-AIPcS<sub>4</sub>, Clip-AIPcS<sub>4</sub>, F127-AIPcS<sub>4</sub>, and AIPcS<sub>4</sub> on SGC-7901 cells. The cells were treated with 0.25–8 μg/mL AuNR-AIPcS<sub>4</sub>, Clip-AIPcS<sub>4</sub>, F127-AIPcS<sub>4</sub>, and AIPcS<sub>4</sub> for 6 hours and incubated again for 24 hours. (D) The antiproliferation activity by AuNR-AIPcS<sub>4</sub>, Clip-AIPcS<sub>4</sub>, F127-AIPcS<sub>4</sub>, and AIPcS<sub>4</sub> on SGC-7901 cells. The cells were treated with AuNR-AIPcS<sub>4</sub>, Clip-AIPcS<sub>4</sub>, F127-AIPcS<sub>4</sub>, and AIPcS<sub>4</sub> at 0.5–8 μg/mL, irradiated by laser light and then incubated continuously for 12 days. After being treated, the cells were fixed with 4% paraformaldehyde, stained with crystal violet, and photographed. (E and F) The colony formation rates were quantified (+ represents irradiation; – represents no irradiation). The experiment was repeated three times. The data represent the average of three experiments and the error bars show SD. \*P<0.05, represents statistical difference in colony formation rate between AIPcS<sub>4</sub> carriers and AIPcS<sub>4</sub>. \*\*P<0.01, represents statistically significant difference in colony formation rate between AIPcS<sub>4</sub> carriers and AIPcS<sub>4</sub>.

**Abbreviations:** AIPcS<sub>4</sub>, Al(III) phthalocyanine chloride tetrasulfonic acid; CCK-8, Cell Counting kit-8; Clip, cationic liposome; RRLAC, arginine-arginine-leucine-alanine-cysteine peptide.

incorporated in Clip-AIPcS<sub>4</sub>, the cell viability dropped to about 20%. But the Clip only increased the anti-growth effect about 3% upon 635 nm laser light irradiation (Figure S5B). Therefore, Clip-AIPcS<sub>4</sub> increased the antitumor effect.

Compared with AuNR-AIPcS<sub>4</sub> and Clip-AIPcS<sub>4</sub>, F127-AIPcS<sub>4</sub> exhibited inferior antitumor growth activities.

Also, F127 drug vector itself retained the high cell viability even at the highest concentration (Figure S5C). In contrast with free AIPcS<sub>4</sub>, the decreasing trend of cell viability was not evident. Notably, F127 demonstrated a slower rate of dissociation and allowed the retention of incorporated drugs for a longer period of time. Thus, the weak anti-growth effect

was speculated to be caused by the slow rate of drug release. To verify this hypothesis, the incubation time of F127–AlPcS<sub>4</sub> on gastric cancer cells was extended to 24 hours, and the dark cytotoxicity and anti-growth effects were reevaluated. The photocytotoxicity significantly increased, whereas the cytotoxicity slightly increased. As shown in [Figure S7](#), at the 8 µg/mL AlPcS<sub>4</sub> concentration, the cell viability under irradiation by laser light was decreased to 23% and the cell viability without irradiation by laser light was only decreased to 87%. Thus, F127–AlPcS<sub>4</sub> is suitable to deliver AlPcS<sub>4</sub> and has excellent PDT effect on gastric cancer cells for prolonged treatments.

To evaluate the contribution of the PTT on the photocytotoxic activity by drug carriers themselves, the temperature variation of AuNR, Clip, and F127 with laser irradiation for 5 minutes was measured. Under the 808 nm laser irradiation, temperature increased by about 8°C for AuNR. Whereas, under the 635 nm laser irradiation, neither Clip or F127 induced the temperature increase ([Figure S8](#)). Hence, the antitumor effect of AuNR–AlPcS<sub>4</sub> was dependent on both the PDT and PTT effects, and Clip–AlPcS<sub>4</sub> and F127–AlPcS<sub>4</sub> were mainly dependent on the PDT effects.

## Antiproliferation activity of different drug delivery systems of AlPcS<sub>4</sub>

Antiproliferative ability is another significant evaluation index for therapeutic effect. To assess the antiproliferative ability of these novel AlPcS<sub>4</sub> carriers, a colony formation assay was performed. As shown in [Figure 2D–F](#), AuNR–AlPcS<sub>4</sub>, Clip–AlPcS<sub>4</sub>, and F127–AlPcS<sub>4</sub> have a strong antiproliferative effect on SGC-7901 cells. The inhibition of the proliferation using AuNR–AlPcS<sub>4</sub> and Clip–AlPcS<sub>4</sub> was excellent, in contrast with that of F127–AlPcS<sub>4</sub>. After 12 days of treatment with AuNR–AlPcS<sub>4</sub> and Clip–AlPcS<sub>4</sub> at 2 µg/mL, after irradiation, SGC-7901 cells were nearly completely inhibited and the percentage of colony formation decreased to nearly 30%. After further increase of treatment concentration, the percentage of colony formation decreased to ~10%. Because of prolonged incubation time for cells during the colony formation assay, the antiproliferative abilities of AuNR–AlPcS<sub>4</sub>, Clip–AlPcS<sub>4</sub>, and F127–AlPcS<sub>4</sub> were also evaluated at repeated drug treatments. All exhibited complete inhibition even at 0.5 µg/mL concentration.

## Fluorescence intensity assay and fluorescence imaging of different AlPcS<sub>4</sub> delivery systems

The above results showed that the synthesized AlPcS<sub>4</sub> delivery systems had significant and different anti-growth effects

on gastric cancer cells. To determine the reason behind the variability, a fluorescence intensity assay was performed in cells treated with different AlPcS<sub>4</sub> carriers. AuNR–AlPcS<sub>4</sub>, Clip–AlPcS<sub>4</sub>, and F127–AlPcS<sub>4</sub> exhibited excellent drug delivery efficiency on gastric cancer cells compared with free AlPcS<sub>4</sub> ([Figure 3](#)) – only <2.5% free AlPcS<sub>4</sub> could be internalized into gastric cancer cells ([Figure 3B](#)). With the help of F127 and Clip vectors, the efficiency of cellular internalization of 8 µg/mL AlPcS<sub>4</sub> increased to 19.7% and 28.4%, respectively ([Figure 3C and D](#)). In addition, the results showed that the fluorescence intensity and the trend of increasing cellular internalization efficiency increased in a dose-dependent manner. The fluorescence intensity was strongly linearly correlated with each concentration, with a correlation coefficient of 0.975 for F127–AlPcS<sub>4</sub> and 0.9676 for Clip–AlPcS<sub>4</sub> ([Figure 3C1 and D1](#)). The fluorescence intensity and the trend of increasing cellular internalization efficiency of Clip–AlPcS<sub>4</sub> were stronger than those of F127–AlPcS<sub>4</sub>, possibly due to a difference in drug-release rate. To confirm this assumption, the fluorescence intensity of AlPcS<sub>4</sub> incubated with F127–AlPcS<sub>4</sub> for 24 hours was evaluated. At 8 µg/mL AlPcS<sub>4</sub>, the fluorescence intensity increased to 1,944 AU ([Figure S9](#)), and the corresponding efficiency of cellular internalization increased to 33.9%. However, for 8 µg/mL free AlPcS<sub>4</sub>, the fluorescence intensity increased only to 720 AU and the corresponding efficiency of cellular internalization increased only by 8.9% ([Figure S9](#)). Hence, Pluronic F127 block copolymer provides excellent AlPcS<sub>4</sub> delivery efficiency for a prolonged period.

As shown in [Figure 3](#), AuNR–AlPcS<sub>4</sub> appears to have a weaker AlPcS<sub>4</sub> delivery efficiency than Clip–AlPcS<sub>4</sub> and F127–AlPcS<sub>4</sub>. The release of AlPcS<sub>4</sub> from the AuNR surface was mainly dependent on heating, resulting in the recovery of the quenched fluorescence. Hence, the recovery fluorescence intensity could be related to heat generation during 808 nm laser light illumination. Undoubtedly, the heat generation effect was influenced by the light illumination time. Thus, we evaluated the relationship between fluorescence intensity and light illumination time. The results revealed that fluorescence intensity increased following prolonged light illumination time ([Figure S6](#)). After irradiation for 10 minutes, the fluorescence intensity was almost completely recovered. In other words, AlPcS<sub>4</sub> was almost completely released from the AuNR surface. After irradiation for 5 minutes, the fluorescence intensity was recovered to nearly 85%. In consideration of the cell survival environment factor, cell viability may be decreased at room temperature. Hence, in this study, the choice of 808 nm laser irradiation time was 5 minutes. The fluorescence intensity of 8 µg/mL AlPcS<sub>4</sub> increased

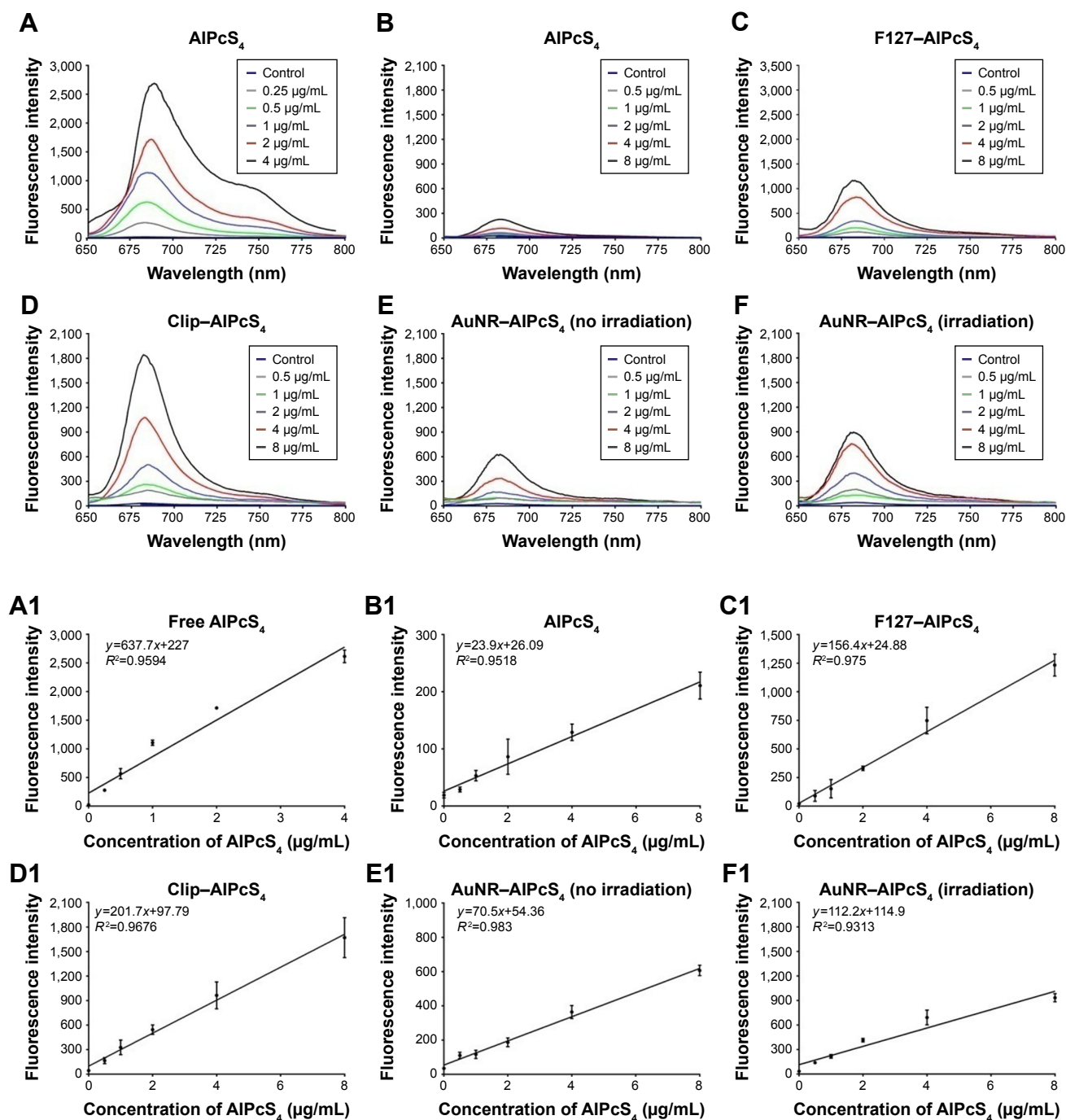


**Figure 3** Evaluation of delivery efficiency of AIPcS<sub>4</sub> carriers in SGC-7901 cells.

**Notes:** (A–F) Total fluorescence intensity of free AIPcS<sub>4</sub> at 0.25–4 μg/mL in cell solution (A) and intracellular fluorescence intensity of AIPcS<sub>4</sub> (B), F127–AIPcS<sub>4</sub> (C), Clip–AIPcS<sub>4</sub> (D), AuNR–AIPcS<sub>4</sub> without irradiation by 808 nm laser light (E), and AuNR–AIPcS<sub>4</sub> with irradiation by 808 nm laser light (F) at 0.5–8 μg/mL after treatment on SGC-7901 cells for 6 hours, respectively. (A1–F1) The correlation between concentration and fluorescence intensity of free AIPcS<sub>4</sub> (without uptake in cells, A1), AIPcS<sub>4</sub> (uptake in cells, B1), F127–AIPcS<sub>4</sub> (uptake in cells, C1), Clip–AIPcS<sub>4</sub> (uptake in cells, D1), AuNR–AIPcS<sub>4</sub> (uptake in cells and without irradiation by 808 nm laser light, E1), and AuNR–AIPcS<sub>4</sub> (uptake in cells with irradiation by 808 nm laser light, F1), respectively. The experiment was repeated three times. The data represent the average of three experiments and the error bars show SD.

**Abbreviations:** AIPcS<sub>4</sub>, Al(III) phthalocyanine chloride tetrasulfonic acid; AuNR, gold nanorods; Clip, cationic liposome.

after irradiation from 627.6 to 898.4 AU (Figure 3E and F). We further tested the fluorescence intensity of AuNR–AIPcS<sub>4</sub> at different time points after being irradiated in cells. Results showed that the fluorescence intensity increased as time was

increased. At 8 μg/mL AIPcS<sub>4</sub>, the fluorescence intensity further increased to 1,299 AU (Figure S4). Self-quenching fluorescence was roughly recovered with AIPcS<sub>4</sub> released from the AuNR surface. Hence, the ultimate corresponding

efficiency of cellular internalization was 21%. In other words, the AIPcS<sub>4</sub> delivery efficiency of AuNR–AIPcS<sub>4</sub> was actually higher than that of F127–AIPcS<sub>4</sub>. However, the linear correlation between fluorescence intensity and AIPcS<sub>4</sub> concentration slightly decreased after 808 nm laser light irradiation, whereby the correlation coefficient decreased from 0.983 to 0.9313, indicating that the release of AIPcS<sub>4</sub> from the AuNR surface and its delivery in cells are complex (Figure 3E1 and F1).

Fluorescence imaging can be used to reveal fluorescence intensity, and thus, it was further evaluated. As shown in Figure 4, the weakest fluorescence signals are observed at 4, 0.5, 1, and 0.5 μg/mL in free AIPcS<sub>4</sub>, Clip–AIPcS<sub>4</sub>, F127–AIPcS<sub>4</sub>, and AuNR–AIPcS<sub>4</sub>, respectively. Obvious fluorescence signal could be observed at 2, 8, and 4 μg/mL in Clip–AIPcS<sub>4</sub>, F127–AIPcS<sub>4</sub>, and AuNR–AIPcS<sub>4</sub>, respectively. After irradiation with an 808 nm laser light, the weakest and relatively obvious fluorescence signals of

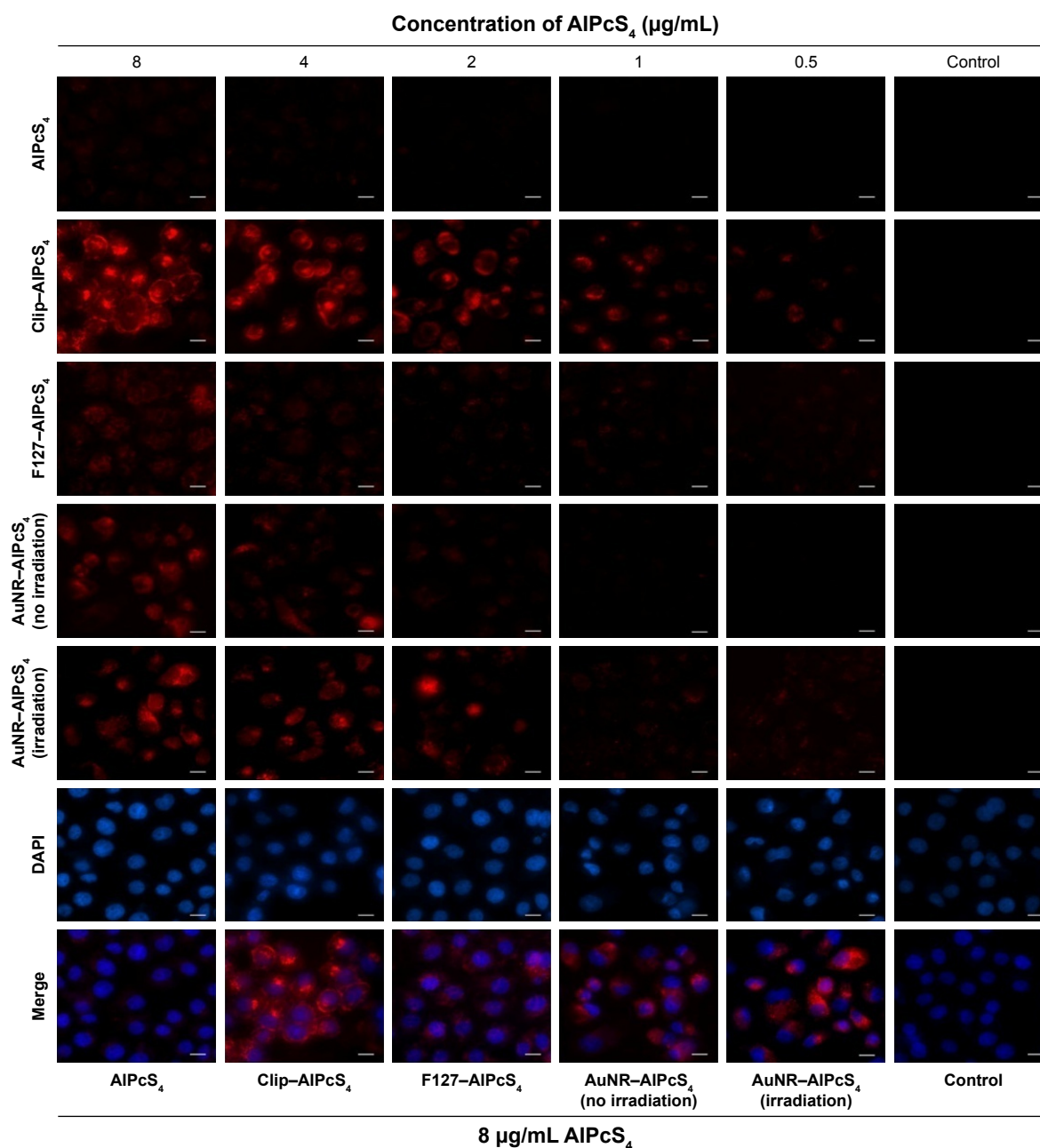


**Figure 4** Fluorescence imaging of delivery efficiency of AIPcS<sub>4</sub> carriers in SGC-7901 cells.

**Notes:** In vitro live cells staining with AIPcS<sub>4</sub>, Clip–AIPcS<sub>4</sub>, F127–AIPcS<sub>4</sub>, and AuNR–AIPcS<sub>4</sub> before and after irradiation by 808 nm laser light, at 0.5–8 μg concentration, and further fluorescence location assay in SGC-7901 cells by staining with DAPI (nuclear staining) and AIPcS<sub>4</sub> at 8 μg. Scale bars =20 μm.

**Abbreviations:** AIPcS<sub>4</sub>, Al(III) phthalocyanine chloride tetrasulfonic acid; AuNR, gold nanorods; Clip, cationic liposome.

AuNR–AIPcS<sub>4</sub> could be observed at 0.5 and 2 μg/mL, respectively. Fluorescence signals increased as AIPcS<sub>4</sub> concentration increased. The Clip–AIPcS<sub>4</sub> and irradiated AuNR–AIPcS<sub>4</sub> fluorescence signals were higher than those of F127–AIPcS<sub>4</sub>. These results were consistent with the fluorescence intensity assay described previously. Apart from the efficiency of cellular internalization, the intracellular locations of the photosensitizer are also another significant factor that influences PDT activities.<sup>60</sup> Fluorescence imaging was used to reveal the intracellular locations and fluorescence change of AIPcS<sub>4</sub> in cells. As shown at the bottom of Figure 4, intense cytoplasmic staining was exhibited in Clip–AIPcS<sub>4</sub>, F127–AIPcS<sub>4</sub>, and AuNR–AIPcS<sub>4</sub>. After increasing the incubation time of F127–AIPcS<sub>4</sub> to 24 hours, the fluorescence signal significantly increased and the intracellular staining remained intense mainly in the cytoplasm but exhibited an increasing shift toward nuclear staining (Figure S10). In summary, AuNR–AIPcS<sub>4</sub>, Clip–AIPcS<sub>4</sub>, and F127–AIPcS<sub>4</sub> increased AIPcS<sub>4</sub> delivery efficiency without influencing the intracellular location. Moreover, Clip–AIPcS<sub>4</sub> cellular internalization efficiency was comparatively optimal.

### Binding affinity of different AIPcS<sub>4</sub> delivery systems to serum proteins

High binding affinity of AIPcS<sub>4</sub> to serum proteins is an important factor to induce low cellular internalization and may lead to decreased AIPcS<sub>4</sub> delivery efficiency and unsatisfactory PDT therapeutic effects on gastric cancer.<sup>23</sup> Hence, evaluating the inhibitory effect of AIPcS<sub>4</sub> with the help of drug carriers is important. Due to the changes in surface charge with the help of drug vectors, the effect of serum proteins on AIPcS<sub>4</sub> should be improved. As shown in Figure 5, in contrast with free AIPcS<sub>4</sub>, the AuNR–AIPcS<sub>4</sub>, Clip–AIPcS<sub>4</sub>, and F127–AIPcS<sub>4</sub> were slightly affected by serum concentration, resulting in improved cellular uptake in gastric cancer cells. Specifically, the inhibition rate of Clip–AIPcS<sub>4</sub> is low. Even in the presence of 20% FBS, the inhibition rate remained <20%. The inhibition rate of AuNR–AIPcS<sub>4</sub> is slightly increased compared with Clip–AIPcS<sub>4</sub>. However, in the presence of 20% FBS, the inhibition rate remained <25%. Among the three systems, only F127–AIPcS<sub>4</sub> had approximately 30% inhibition rate in the presence of 20% FBS, and compared with free AIPcS<sub>4</sub>, its inhibition of binding affinity to FBS was still increased by 10%. The results of binding affinity to serum proteins were consistent with the results on the zeta potential of AuNR–AIPcS<sub>4</sub>, Clip–AIPcS<sub>4</sub>, and F127–AIPcS<sub>4</sub>. The results revealed that serum proteins exhibited high affinity to negatively charged molecules. Hence,

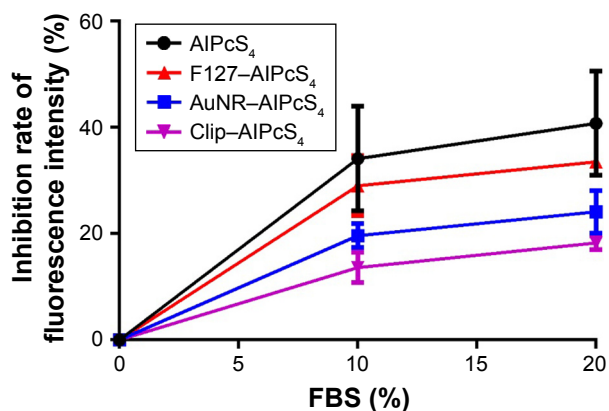


**Figure 5** Inhibition effect on the binding affinity of AIPcS<sub>4</sub> to FBS with F127, AuNR, and Clip.

**Notes:** Inhibition rate analysis and comparison of fluorescence intensity of AIPcS<sub>4</sub>, F127–AIPcS<sub>4</sub>, AuNR–AIPcS<sub>4</sub>, and Clip–AIPcS<sub>4</sub> at 8 μg/mL with the presence of 10% FBS and 20% FBS in the medium. The experiment was tested in triplicate. The data represent the average of three experiments and the bar is SD.

**Abbreviations:** AIPcS<sub>4</sub>, Al(III) phthalocyanine chloride tetrasulfonic acid; AuNR, gold nanorods; Clip, cationic liposome; FBS, fetal bovine serum.

changing or reducing the negative charge of AIPcS<sub>4</sub> may be conducive for the delivery of AIPcS<sub>4</sub> and the enhancement of antitumor therapy effects.

### Apoptosis and necrosis induced by different drug delivery systems of AIPcS<sub>4</sub>

Fluorescence imaging of AIPcS<sub>4</sub> showed that the morphology of the cell nucleus changed after the treatments. Cell enlargement and rupture as the typical necrosis characteristics, or cell shrinkage and nuclear fragmentation as the representative apoptotic characteristics occurred after treatments with F127–AIPcS<sub>4</sub>, Clip–AIPcS<sub>4</sub>, and AuNR–AIPcS<sub>4</sub>. The death of gastric cancer cells may be induced by apoptosis and necrosis in PDT.<sup>10,11,61</sup> Clarifying whether or not it activates apoptosis or necrosis to induce gastric cancer cell death and further illuminating the relationship between apoptosis and necrosis induced by modified AIPcS<sub>4</sub>-PDT may help regulate these processes and potentiate the anti-growth effects. Hence, we evaluated apoptosis and necrosis using Hoechst 33258/PI staining and flow cytometry. As shown in Figure 6, SGC-7901 cells showed apparent apoptotic characteristics after treatment with AuNR–AIPcS<sub>4</sub>, Clip–AIPcS<sub>4</sub>, or F127–AIPcS<sub>4</sub> and irradiation. Free AIPcS<sub>4</sub> also led to slight apoptosis. Moreover, Clip–AIPcS<sub>4</sub> led to apoptosis that was more potent than that in AuNR–AIPcS<sub>4</sub> and F127–AIPcS<sub>4</sub>. Upon exposure to 8 μg/mL AIPcS<sub>4</sub> incorporated with AuNR–AIPcS<sub>4</sub>, Clip–AIPcS<sub>4</sub>, or F127–AIPcS<sub>4</sub>, the percent of apoptotic bodies reached 56%, 69%, and 17%, respectively, through Hoechst staining analysis (Figure S11), and the early apoptotic cells reached 27.9%, 30.3%, and 7.5%, respectively, through flow cytometry

analysis (Figure 6). We further demonstrated the apoptosis induced using different AIPc<sub>4</sub> delivery vectors with dosage variations. Results showed that apoptotic bodies decreased as the dosage decreased. Due to the cell membrane integrity being broken during cell necrosis, the necrotic cells can be stained with PI staining dye, which cannot cross the membrane of live cells. The results of PI-stained cells showed that Clip-AIPc<sub>4</sub>, F127-AIPc<sub>4</sub>, and AIPc<sub>4</sub> lead to slight necrosis compared with apoptosis. However, with the increased concentration, the percentage of necrotic cells increased – 36%, 32%, and 21% were obtained through Hoechst/PI staining analysis (Figure S11) and 36.2%, 21.4%, and 8.5% late apoptotic and necrotic cells were obtained through flow cytometry analysis at 8 μg/mL for AuNR-AIPc<sub>4</sub>, Clip-AIPc<sub>4</sub>, and F127-AIPc<sub>4</sub>, respectively. Numerous secondary necrotic cells (cells not only exhibiting typical apoptotic features but also showing the hallmark of cell membrane dysfunction features)

were exhibited after PDT therapy of AuNR-AIPc<sub>4</sub> and Clip-AIPc<sub>4</sub> in the Hoechst and PI staining images. Generally, the apoptosis and necrosis results measured by Hoechst/PI staining are basically consistent with the results determined by flow cytometry. The percentage of apoptosis/necrosis comes from flow cytometry is lower than that in Hoechst/PI staining analysis. This may be caused by not all cells irradiated by laser light (the spot size [2.5×3 cm] is less than the size of the culture dish [3.1×3.1 cm]). Compared with the results of apoptosis and necrosis, the induced late apoptotic ability and necrotic ability of F127-AIPc<sub>4</sub> were more effective than the induced early apoptotic ability. Thus, we further evaluated the death of F127-AIPc<sub>4</sub> at a 24-hour incubation time. The late apoptotic cells and necrotic cells induced by F127-AIPc<sub>4</sub> were still higher in number than the early apoptotic cells (Figure S12). Generally, with the help of drug delivery vectors, AIPc<sub>4</sub> induces gastric cancer cell death mainly through apoptosis.

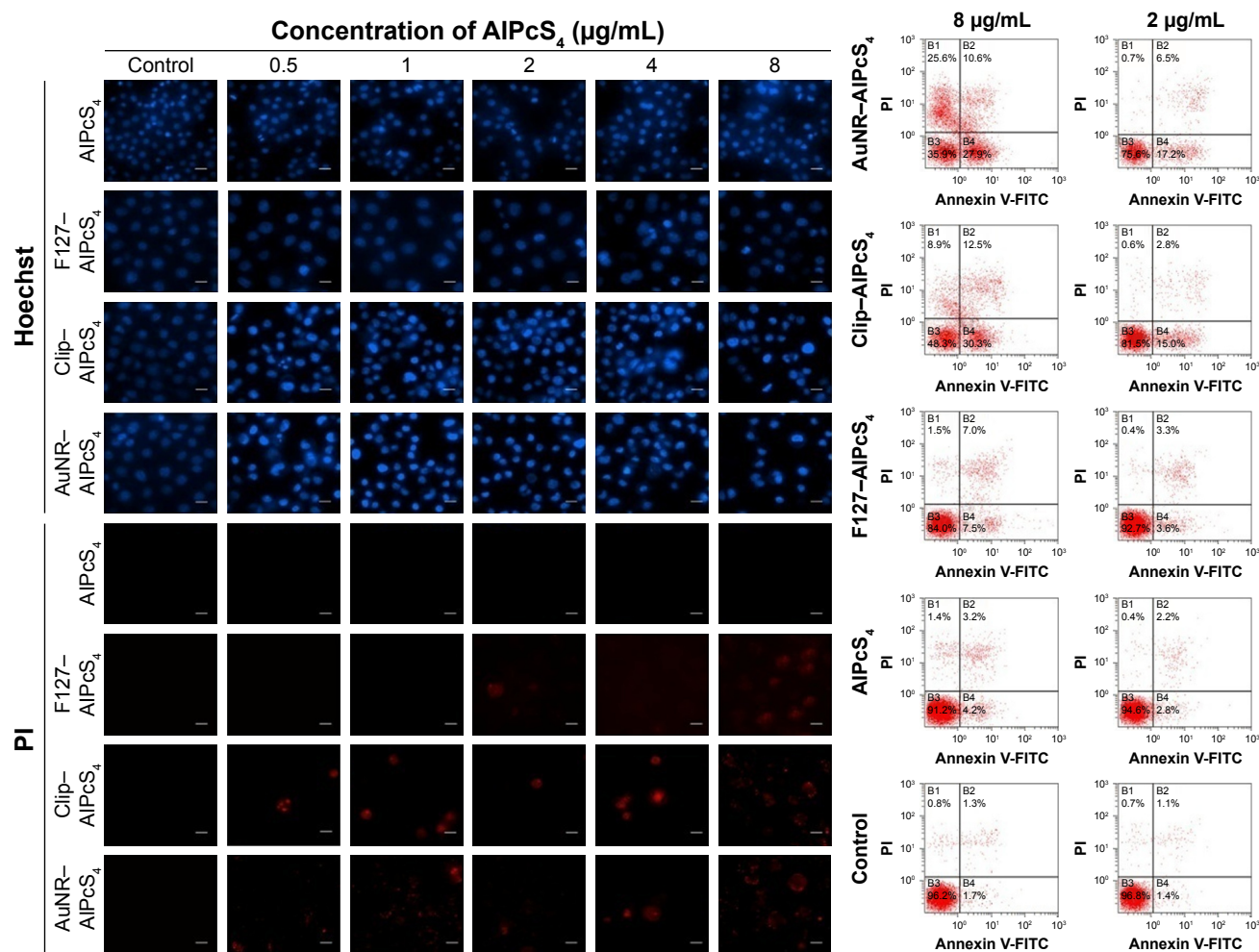


**Figure 6** Apoptosis and necrosis induced by AIPc<sub>4</sub>, F127-AIPc<sub>4</sub>, Clip-AIPc<sub>4</sub>, and AuNR-AIPc<sub>4</sub> in gastric cancer cells.

**Notes:** SGC-7901 cells treated with AIPc<sub>4</sub>, F127-AIPc<sub>4</sub>, Clip-AIPc<sub>4</sub>, and AuNR-AIPc<sub>4</sub> at 0.5–8 μg/mL were irradiated, incubated for 24 hours, stained with Hoechst 33258 and PI dyes and then imaged. All the Hoechst and PI stain images were acquired at 40× magnification. Scale bars =20 μm.

**Abbreviations:** AIPc<sub>4</sub>, Al(III) phthalocyanine chloride tetrasulfonic acid; AuNR, gold nanorods; Clip, cationic liposome; PI, propidium iodide.

Low-dose PDT has been revealed to induce apoptosis, whereas the ability of the high-dose PDT to cause necrosis has already been demonstrated. Hence, F127–AlPc<sub>4</sub>, Clip–AlPc<sub>4</sub>, and AuNR–AlPc<sub>4</sub> can be considered as low-dose PDT that causes low-toxicity side effects on normal organs.

## SOG and ROS production by different drug delivery systems of AlPc<sub>4</sub>

The photosensitizer-generated SOG or ROS is a predominant influence that damages cellular organelles and membranes and further induces cell death in PDT therapy.<sup>61</sup> Therefore, we measured the concentrations of SOG and ROS in SGC-7901 cells induced by the synthesized AlPc<sub>4</sub> delivery vectors or free AlPc<sub>4</sub> and compared their differences. As shown in Figure 7, compared with free AlPc<sub>4</sub>, the concentration of SOSGR induced by AuNR–AlPc<sub>4</sub>, Clip–AlPc<sub>4</sub>, and F127–AlPc<sub>4</sub> increased at average levels of 11-fold, five-fold, and three-fold, respectively. The increasing

trend of SOSGR of AuNR–AlPc<sub>4</sub> was the most pronounced. This may be caused by AuNR, which enhanced the AlPc<sub>4</sub> delivery efficiency and SOG generation by itself (Figure 7A). Similar behaviors were obtained in the research of Vankayala et al and Huang et al.<sup>62,63</sup> This can be verified by the increasing trend of SOSGR on AuNR–AlPc<sub>4</sub> being the most pronounced; however, the fluorescence intensity of AuNR–AlPc<sub>4</sub> increased slightly. On the other hand, the DCFH-DA fluorescence intensity representing ROS also exhibited a significant increase. Compared with the free AlPc<sub>4</sub>, the AuNR–AlPc<sub>4</sub>, Clip–AlPc<sub>4</sub>, and F127–AlPc<sub>4</sub> resulted in highly significant increases. Furthermore, at values <2 μg/mL AlPc<sub>4</sub>, no significant difference was found on the increasing trend among them; however, the increasing trend of AuNR–AlPc<sub>4</sub> was higher than those of Clip–AlPc<sub>4</sub> and F127–AlPc<sub>4</sub> with increased concentration values. At the highest concentration of AlPc<sub>4</sub>, the fluorescence intensity of ROS induced AuNR–AlPc<sub>4</sub>,

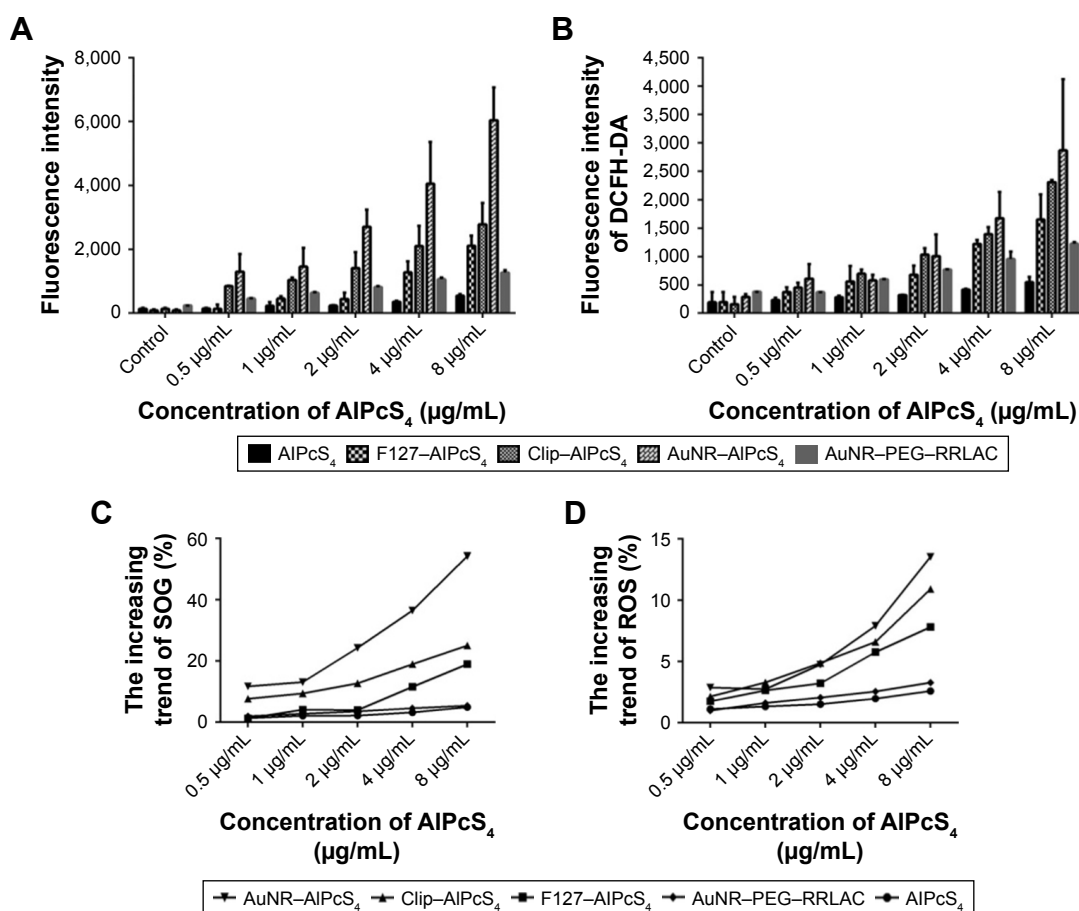


**Figure 7** SOG and ROS production in SGC-7901 cells treated with AlPc<sub>4</sub> carriers or AlPc<sub>4</sub>.

**Notes:** (A, B) The fluorescence intensity of SOSGR probe or DCFH-DA probe measured to analyze SOG and ROS production in SGC-7901 cells treated with AlPc<sub>4</sub>, F127–AlPc<sub>4</sub>, Clip–AlPc<sub>4</sub>, AuNR–AlPc<sub>4</sub>, and AuNR–PEG–RRLAC and irradiated with laser light, at different concentrations (0.5–8 μg/mL). Data represent the average of three experiments and the bar is SD. (C and D) The relative increased trend of SOG and ROS production in SGC-7901 cells treated with AlPc<sub>4</sub>, F127–AlPc<sub>4</sub>, Clip–AlPc<sub>4</sub>, and AuNR–AlPc<sub>4</sub> and irradiated with laser light, at different concentrations (0.5–8 μg/mL).

**Abbreviations:** AlPc<sub>4</sub>, Al(III) phthalocyanine chloride tetrasulfonic acid; AuNR, gold nanorods; Clip, cationic liposome; DCFH-DA, 2',7'-Dichlorodihydrofluorescein diacetate; ROS, reactive oxygen species; RRLAC, arginine-arginine-leucine-alanine-cysteine peptide; SOG, singlet oxygen; SOSGR, singlet oxygen sensor green reagent.

Clip-AIPcS<sub>4</sub>, and F127-AIPcS<sub>4</sub> to increase at average levels of 10.9-fold, 7.8-fold, and 2.5-fold, respectively. Higher levels generated by AuNR-AIPcS<sub>4</sub> was not only for the increased concentration of accumulated AIPcS<sub>4</sub> in the cells but AuNR carriers alone can induce ROS accumulation.<sup>64</sup>

### Mitochondrial transmembrane potential changes induced by different drug delivery systems of AIPcS<sub>4</sub>

The mitochondria play a central role in apoptosis.<sup>65</sup> One of the reasons is that a photosensitizer can be accumulated in the mitochondria and local damage is induced by photosensitization and may be propagated to the mitochondria by various means.<sup>66</sup> AIPcS<sub>4</sub>-PDT may induce mitochondrial dysfunction and decrease the mitochondrial membrane potential to

activate apoptosis.<sup>67,68</sup> The  $\Delta\Psi_m$  loss is a flag for apoptosis and which can release apoptotic factors to induce cellular dysfunction and cell death. Hence, the change of  $\Delta\Psi_m$  was detected by using JC-1 dye, which could aggregate in normal mitochondria and exhibit red fluorescence. By altering  $\Delta\Psi_m$ , the accumulation of JC-1 was prevented, and JC-1 in monomer form was dispersed throughout the cells, thereby leading to a shift from red to green fluorescence. Moreover, the treated SGC-7901 cells showed obvious green fluorescence after irradiation and fluorescence increased further after 16 hours. Also, the green fluorescence signals of F127-AIPcS<sub>4</sub>, AuNR-AIPcS<sub>4</sub>, and Clip-AIPcS<sub>4</sub> were higher than that of the free AIPcS<sub>4</sub>, indicating more potent apoptotic activity with the help of drug delivery vectors (Figure 8A). The ratio of red fluorescence to green fluorescence was

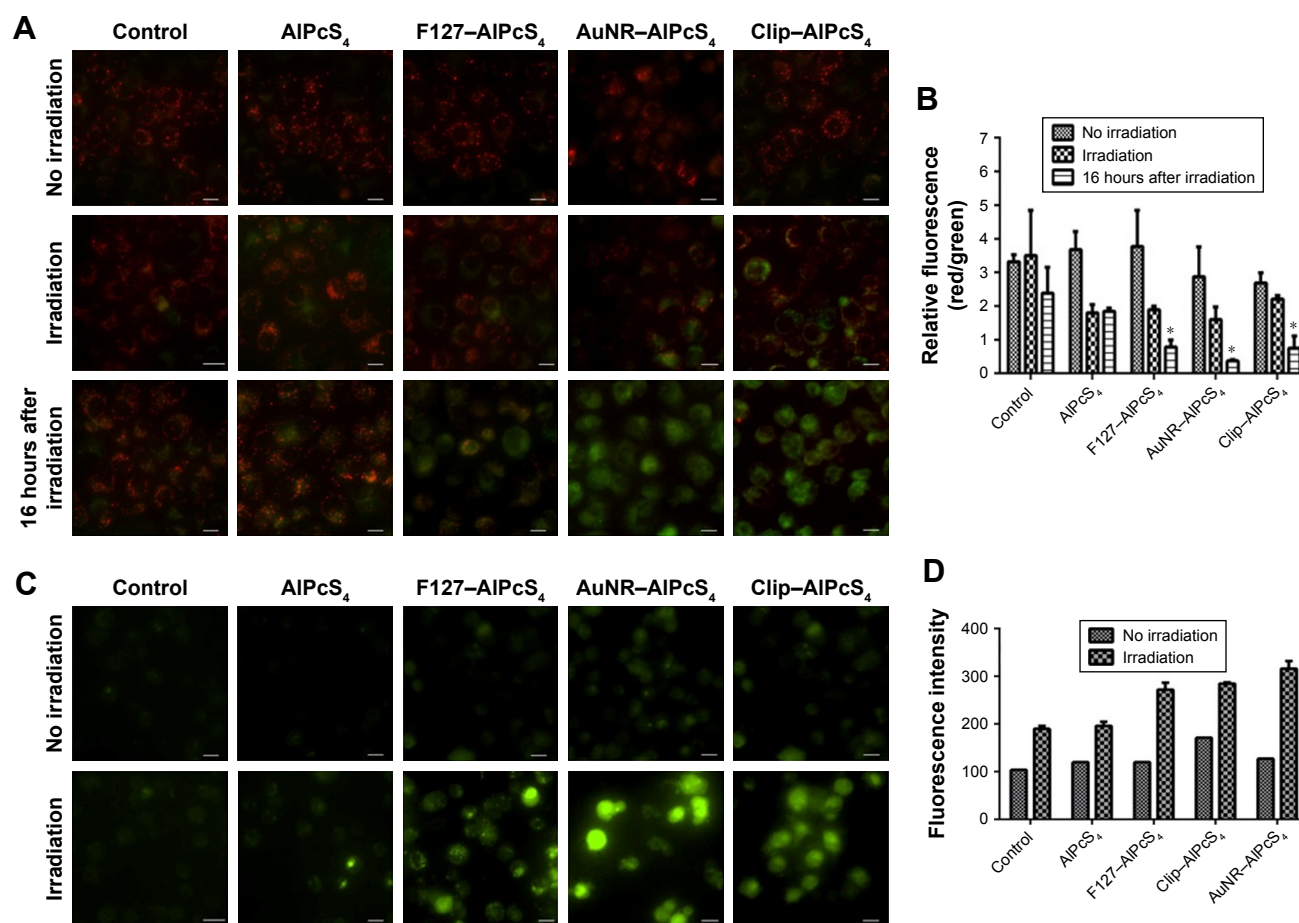


**Figure 8** The loss of mitochondrial transmembrane potential ( $\Delta\Psi_m$ ) and ( $Ca^{2+}$ ) overload induced by different AIPcS<sub>4</sub> carriers or AIPcS<sub>4</sub> before and after PDT therapy. **Notes:** (A) The  $\Delta\Psi_m$  change in SGC-7901 cells after treatment with AIPcS<sub>4</sub>, F127-AIPcS<sub>4</sub>, AuNR-AIPcS<sub>4</sub>, and Clip-AIPcS<sub>4</sub> at 8  $\mu$ g/mL was measured by JC-1 reagent without irradiation of laser light, with irradiation of laser light, and after irradiation for 16 hours (left). Red fluorescence represents the mitochondrial aggregate form of JC-1 (JC-1 polymers), which indicates the intact mitochondrial membrane potential. Green fluorescence represents the monomeric form of JC-1 (JC-1 monomers), which indicates the dissipation mitochondrial membrane potential. (B) Ratios of JC-1 polymers to JC-1 monomers (red/green fluorescence) were assessed for no irradiation group, irradiation group, and irradiation group after 16 hours (right). (C) The fluorescence imaging of Fluor/AM probes were measured in SGC-7901 cells treated with AIPcS<sub>4</sub>, F127-AIPcS<sub>4</sub>, AuNR-AIPcS<sub>4</sub>, and Clip-AIPcS<sub>4</sub> at 8  $\mu$ g/mL before and after irradiation with laser light. (D) The corresponding fluorescence intensity assay of Fluor/AM probes was assessed for no irradiation group and irradiation group. The data represent the average of three experiments and the error bars show SD. \* $P < 0.05$ , represents statistical difference between AIPcS<sub>4</sub> carriers and AIPcS<sub>4</sub> or control. Scale bars are 20  $\mu$ m.

**Abbreviations:** AIPcS<sub>4</sub>, Al(III) phthalocyanine chloride tetrasulfonic acid; AuNR, gold nanorods; Clip, cationic liposome; PDT, photodynamic therapy.

further quantified to reveal the difference between drug delivery vectors. The results showed that the red/green fluorescence ratios of F127–AlPcS<sub>4</sub>, AuNR–AlPcS<sub>4</sub>, and Clip–AlPcS<sub>4</sub> decreased from 3.76±1.08, 2.87±0.88, and 2.69±1.08 to 2.89±0.1, 1.6±0.36, and 2.21±1.08, respectively, and further decreased to 0.79±0.15, 0.37.6±0.02, and 0.75±0.15 after 16 hours (Figure 8B). Compared with the control and AlPcS<sub>4</sub>, the loss of ΔΨ<sub>m</sub> was evident, especially after 16 hours of irradiation; moreover, a significant difference between AlPcS<sub>4</sub> conjugated with drug delivery vectors and AlPcS<sub>4</sub> existed. Therefore, AlPcS<sub>4</sub> conjugated with drug delivery vectors has highly preferable apoptosis-inducing ability.

### ([Ca<sup>2+</sup>]<sub>i</sub>) overload induced by different drug delivery systems of AlPcS<sub>4</sub>

([Ca<sup>2+</sup>]<sub>i</sub>) overload plays a key role in cell death both at the early and at the late stages of apoptosis. Increased intracellular Ca<sup>2+</sup> can trigger a rapid release of cytochrome C from the mitochondria and further activate apoptosis.<sup>69</sup> Hence, whether AlPcS<sub>4</sub>, which is conjugated with drug delivery vectors' composite systems, further leads to [Ca<sup>2+</sup>]<sub>i</sub> concentration elevation in SGC-7901 cells during PDT therapy was investigated. Their differences were compared through fluorescence intensity analysis. As shown in Figure 8C, the green fluorescence signal represents that [Ca<sup>2+</sup>]<sub>i</sub> information was evidently increased after treating cells with F127–AlPcS<sub>4</sub>, AuNR–AlPcS<sub>4</sub>, and Clip–AlPcS<sub>4</sub>, compared with the control and free AlPcS<sub>4</sub>. The relative fluorescence intensity of AuNR–AlPcS<sub>4</sub> was slightly higher than those of F127–AlPcS<sub>4</sub> and Clip–AlPcS<sub>4</sub> (Figure 8D). This result was primarily consistent with the apoptosis-inducing ability of the drug. The main goal of our research was to study an effective strategy to increase AlPcS<sub>4</sub>-PDT effects and reduce the AlPcS<sub>4</sub> binding affinity to serum albumin. The exact functional mechanism of AlPcS<sub>4</sub>-PDT and AlPcS<sub>4</sub> for inducing cell death will be investigated at a later date and is currently active in our laboratory. Whether or not apoptosis is induced by death receptor-mediated apoptosis, mitochondria-mediated apoptosis, and endoplasmic reticulum stress-induced apoptosis will be demonstrated by Western blot analysis. Beyond that, using quantum dots, polymer nanoparticles, nanoemulsions, the other types of gold nanomaterials, and so on to improve AlPcS<sub>4</sub> delivery and enhance PDT effect may be another usable strategy on gastric cancer.<sup>35,37,46,70</sup> Especially, it is useful to use tumor-targeting PDT system-based drug delivery carriers in accordance with their functionality modification with

specific tumor-targeting molecules, such as antibodies, peptide, and aptamer.<sup>59,71–74</sup> In our study, AuNR, Clip, and F127 vectors themselves are suited to be functionally modified with specific targeting molecules. Therefore, AlPcS<sub>4</sub> PDT effect may be further improved using AuNR–AlPcS<sub>4</sub>, Clip–AlPcS<sub>4</sub>, and F127–AlPcS<sub>4</sub> with targeting specificity, which will be evaluated in the future. Generally, AuNR, Clip, and F127 are preferable AlPcS<sub>4</sub> delivery vectors for gastric cancer PDT therapy.

## Conclusion

In conclusion, we synthesized a series of AlPcS<sub>4</sub> drug delivery systems based on AuNR with the help of SH–PEG–NHS, Clip, and Pluronic F127 drug delivery vectors to increase the AlPcS<sub>4</sub> delivery efficiency, reduce the binding affinity of AlPcS<sub>4</sub> to serum proteins, and enhance SOG generation, which led to a highly efficient antitumor therapy on gastric cancer cells. Among these, Clip has the optimal AlPcS<sub>4</sub> drug delivery efficiency induced by its higher intracellular bioavailability and low binding affinity to serum proteins. Positively charged AuNR have the best anti-growth effects because of their ability to enhance the drug delivery efficiency of AlPcS<sub>4</sub>, reduce the binding affinity of AlPcS<sub>4</sub> to serum proteins, and induce gastric cancer cell death through photothermal function. AlPcS<sub>4</sub>, with the help of Pluronic F127, has the significant anti-growth effect on gastric cancer cells by extending treatment time while maintaining low dark cytotoxicity on a certain level with AuNR–AlPcS<sub>4</sub> and Clip–AlPcS<sub>4</sub>. Our findings also suggested that AlPcS<sub>4</sub>-PDT modified with AuNR, Clip, or F127 nanomicelles could effectively inhibit the growth and proliferation of gastric cancer cells mainly through apoptosis.

## Acknowledgments

This work was supported by the National Natural Science Foundation of China under grant numbers 61505159, 61575156, 61775178, 61335012, 61727823, and 61705177, and the China Postdoctoral Science Foundation under grant number 2015M572570. The TEM study was undertaken at the International Center for Dielectric Research, Xi'an Jiaotong University, Xi'an, China. The authors thank Mr Chuansheng Ma for his help in using the TEM facility.

## Disclosure

The authors report no conflicts of interest in this work.

## References

1. Torre LA, Bray F, Siegel RL, Ferlay J, Lortet-Tieulent J, Jemal A. Global cancer statistics, 2012. *CA Cancer J Clin.* 2015;65(2):87–108.

2. McCall MD, Graham PJ, Bathe OF. Quality of life: a critical outcome for all surgical treatments of gastric cancer. *World J Gastroenterol*. 2016;22(3):1101–1113.
3. Lee JH, Kim JG, Jung HK, et al. Clinical practice guidelines for gastric cancer in Korea: an evidence-based approach. *J Gastric Cancer*. 2014;14(2):87–104.
4. Yang X, Yang S, Chai H, et al. A novel isoquinoline derivative anti-cancer agent and its targeted delivery to tumor cells using transferrin-conjugated liposomes. *PLoS One*. 2015;10(8):e0136649.
5. Dougherty TJ, Gomer CJ, Henderson BW, et al. Photodynamic therapy. *J National Cancer Institute*. 1998;90(12):889–905.
6. Agostinis P, Berg K, Cengel KA, et al. Photodynamic therapy of cancer: an update. *CA Cancer J Clin*. 2011;61(4):250–281.
7. Vrouenraets MB, Visser GW, Snow GB, van Dongen GA. Basic principles, applications in oncology and improved selectivity of photodynamic therapy. *Anticancer Res*. 2003;23(1B):505–522.
8. Rodriguez ME, Cogno IS, Milla Sanabria LS, Moran YS, Rivarola VA. Heat shock proteins in the context of photodynamic therapy: autophagy, apoptosis and immunogenic cell death. *Photochem Photobiol Sci*. 2016;15(9):1090–1102.
9. Moor AC. Signaling pathways in cell death and survival after photodynamic therapy. *J Photochem Photobiol B*. 2000;57(1):1–13.
10. Mfouo-Tynga I, Abrahamse H. Cell death pathways and phthalocyanine as an efficient agent for photodynamic cancer therapy. *Int J Mol Sci*. 2015;16(5):10228–10241.
11. Mroz P, Yaroslavsky A, Kharkwal GB, Hamblin MR. Cell death pathways in photodynamic therapy of cancer. *Cancers*. 2011;3(2):2516–2539.
12. Gao W, Wang Z, Lv L, et al. Photodynamic therapy induced enhancement of tumor vasculature permeability using an upconversion nanoconstruct for improved intratumoral nanoparticle delivery in deep tissues. *Theranostics*. 2016;6(8):1131–1144.
13. Allison RR, Downie GH, Cuenca R, Hu XH, Childs CJ, Sibata CH. Photosensitizers in clinical PDT. *Photodiagnosis Photodyn Ther*. 2004;1(1):27–42.
14. Rosenthal I. Phthalocyanines as photodynamic sensitizers. *Photochem Photobiol*. 1991;53(6):859–870.
15. Samuni A, Samuni A, Swartz HM. Evaluation of dibromonitrosobenzene sulfonate as a spin trap in biological systems. *Free Radic Biol Med*. 1989;7(1):37–43.
16. da Silva NS, Ribeiro Cde M, Machado AH, Pacheco-Soares C. Ultrastructural changes in *Tritrichomonas foetus* after treatments with AIPc<sub>4</sub> and photodynamic therapy. *Vet Parasitol*. 2007;146(1–2):175–181.
17. Derycke AS, Kamuhabwa A, Gijssens A, et al. Transferrin-conjugated liposome targeting of photosensitizer AIPc<sub>4</sub> to rat bladder carcinoma cells. *J Natl Cancer Inst*. 2004;96(21):1620–1630.
18. Plaetzer K, Kiesslich T, Krammer B, Hammerl P. Characterization of the cell death modes and the associated changes in cellular energy supply in response to AIPc<sub>4</sub>-PDT. *Photochem Photobiol Sci*. 2002;1(3):172–177.
19. Gijssens A, Derycke A, Missiaen L, et al. Targeting of the photocytotoxic compound AIPc<sub>4</sub> to HeLa cells by transferrin conjugated PEG-liposomes. *Int J Cancer*. 2002;101(1):78–85.
20. Ruck A, Heckelsmiller K, Kaufmann R, Grossman N, Haseroth E, Akgun N. Light-induced apoptosis involves a defined sequence of cytoplasmic and nuclear calcium release in AIPc<sub>4</sub>-photosensitized rat bladder RR 1022 epithelial cells. *Photochem Photobiol*. 2000;72(2):210–216.
21. Moor AC, Wagenaars-van Gompel AE, Hermanns RC, et al. Inhibition of various steps in the replication cycle of vesicular stomatitis virus contributes to its photoinactivation by AIPc<sub>4</sub> or Pc<sub>4</sub> and red light. *Photochem Photobiol*. 1999;69(3):353–359.
22. Peng Q, Moan J, Farrants GW, Danielsen HE, Rimington C. Location of P-II and AIPCS<sub>4</sub> in human tumor LOX in vitro and in vivo by means of computer-enhanced video fluorescence microscopy. *Cancer Lett*. 1991;58(1–2):37–47.
23. Jang B, Park JY, Tung CH, Kim IH, Choi Y. Gold nanorod-photosensitizer complex for near-infrared fluorescence imaging and photodynamic/photothermal therapy in vivo. *ACS Nano*. 2011;5(2):1086–1094.
24. Filyasova AI, Kudelina IA, Feofanov AV. A spectroscopic study of the interaction of tetrasulfonated aluminum phthalocyanine with human serum albumin. *J Mol Structure*. 2001;565–566:173–176.
25. Debele TA, Peng S, Tsai HC. Drug carrier for photodynamic cancer therapy. *Int J Mol Sci*. 2015;16(9):22094–22136.
26. Sawant RR, Torchilin VP. Liposomes as ‘smart’ pharmaceutical nano-carriers. *Soft Matter*. 2010;6(17):4026–4044.
27. Jiang F, Lilje L, Grenier J, Li Y, Wilson MD, Chopp M. Photodynamic therapy of U87 human glioma in nude rat using liposome-delivered photofrin. *Lasers Surg Med*. 1998;22(2):74–80.
28. Jiang F, Lilje L, Logie B, Li Y, Chopp M. Photodynamic therapy of 9L gliosarcoma with liposome-delivered photofrin. *Photochem Photobiol*. 1997;65(4):701–706.
29. Lilje L, Wilson BC. Photodynamic therapy of intracranial tissues: a preclinical comparative study of four different photosensitizers. *J Clin Laser Med Surg*. 1998;16(2):81–91.
30. Chen K, Preuss A, Hackbarth S, Wacker M, Langer K, Roder B. Novel photosensitizer-protein nanoparticles for photodynamic therapy: photophysical characterization and in vitro investigations. *J Photochem Photobiol B*. 2009;96(1):66–74.
31. Lee SJ, Park K, Oh YK, et al. Tumor specificity and therapeutic efficacy of photosensitizer-encapsulated glycol chitosan-based nanoparticles in tumor-bearing mice. *Biomaterials*. 2009;30(15):2929–2939.
32. Yoon HY, Koo H, Choi KY, et al. Tumor-targeting hyaluronic acid nanoparticles for photodynamic imaging and therapy. *Biomaterials*. 2012;33(15):3980–3989.
33. Park H, Na K. Conjugation of the photosensitizer Chlorin e6 to pluronic F127 for enhanced cellular internalization for photodynamic therapy. *Biomaterials*. 2013;34(28):6992–7000.
34. Tang W, Xu H, Park EJ, Philbert MA, Kopelman R. Encapsulation of methylene blue in polyacrylamide nanoparticle platforms protects its photodynamic effectiveness. *Biochem Biophys Res Commun*. 2008;369(2):579–583.
35. Li L, Zhao JF, Won N, Jin H, Kim S, Chen JY. Quantum dot-aluminum phthalocyanine conjugates perform photodynamic reactions to kill cancer cells via fluorescence resonance energy transfer. *Nanoscale Res Lett*. 2012;7(1):386.
36. Jang B, Choi Y. Photosensitizer-conjugated gold nanorods for enzyme-activatable fluorescence imaging and photodynamic therapy. *Theranostics*. 2012;2(2):190–197.
37. Muehlmann LA, Ma BC, Longo JP, Almeida Santos Mde F, Azevedo RB. Aluminum-phthalocyanine chloride associated to poly(methyl vinyl ether-co-maleic anhydride) nanoparticles as a new third-generation photosensitizer for anticancer photodynamic therapy. *Int J Nanomed*. 2014;9:1199–1213.
38. Erbas S, Gorgulu A, Kocakusakogullari M, Akkaya EU. Non-covalent functionalized SWNTs as delivery agents for novel Bodipy-based potential PDT sensitizers. *Chem Commun (Camb)*. 2009;(33):4956–4958.
39. Zhang Z, Wang S, Xu H, Wang B, Yao C. Role of 5-aminolevulinic acid-conjugated gold nanoparticles for photodynamic therapy of cancer. *J Biomed Opt*. 2015;20(5):51043.
40. Xu H, Liu C, Mei J, et al. Effects of light irradiation upon photodynamic therapy based on 5-aminolevulinic acid-gold nanoparticle conjugates in K562 cells via singlet oxygen generation. *Int J Nanomedicine*. 2012;7:5029–5038.
41. Master A, Livingston M, Sen Gupta A. Photodynamic nanomedicine in the treatment of solid tumors: perspectives and challenges. *J Control Release*. 2013;168(1):88–102.
42. Mooney R, Roma L, Zhao D, et al. Neural stem cell-mediated intratumoral delivery of gold nanorods improves photothermal therapy. *ACS Nano*. 2014;8(12):12450–12460.
43. Guo J, Rahme K, He Y, Li LL, Holmes JD, O’Driscoll CM. Gold nanoparticles enlighten the future of cancer theranostics. *Int J Nanomed*. 2017;12:6131–6152.
44. Parida S, Maiti C, Rajesh Y, et al. Gold nanorod embedded reduction responsive block copolymer micelle-triggered drug delivery combined with photothermal ablation for targeted cancer therapy. *Biochim Biophys Acta*. 2017;1861(1 Pt A):3039–3052.

45. Ran R, Liu Y, Gao H, et al. Enhanced gene delivery efficiency of cationic liposomes coated with PEGylated hyaluronic acid for anti P-glycoprotein siRNA: a potential candidate for overcoming multi-drug resistance. *Int J Pharm*. 2014;477(1–2):590–600.
46. Young J, Yee M, Kim H, et al. Phototoxicity of liposomal Zn- and Al-phthalocyanine against cervical and oral squamous cell carcinoma cells in vitro. *Med Sci Monit Basic Res*. 2016;22:156–164.
47. Li Y, Wang J, Gao Y, Zhu J, Wientjes MG, Au JL. Relationships between liposome properties, cell membrane binding, intracellular processing, and intracellular bioavailability. *AAPS J*. 2011;13(4):585–597.
48. Ibrahim S, Tagami T, Ozeki T. Effective-loading of platinum-chloroquine into PEGylated neutral and cationic liposomes as a drug delivery system for resistant malaria parasites. *Biol Pharm Bull*. 2017;40(6):815–823.
49. Han HD, Byeon Y, Jeon HN, Shin BC. Enhanced localization of anticancer drug in tumor tissue using polyethylenimine-conjugated cationic liposomes. *Nanoscale Res Lett*. 2014;9(1):209.
50. Zhao T, Liu X, Li Y, et al. Fluorescence and drug loading properties of ZnSe:Mn/ZnS-Paclitaxel/SiO<sub>2</sub> nanocapsules templated by F127 micelles. *J Colloid Interface Sci*. 2017;490:436–443.
51. Al Khateb K, Ozhmukhametova EK, Mussin MN, et al. In situ gelling systems based on Pluronic F127/Pluronic F68 formulations for ocular drug delivery. *Int J Pharm*. 2016;502(1–2):70–79.
52. Yuan A, Yang B, Wu J, Hu Y, Ming X. Dendritic nanoconjugates of photosensitizer for targeted photodynamic therapy. *Acta Biomater*. 2015;21:63–73.
53. Liang S, Lin T, Ding J, et al. Screening and identification of vascular-endothelial-cell-specific binding peptide in gastric cancer. *J Mol Med (Berl)*. 2006;84(9):764–773.
54. Ke Y, Ning T, Wang B. [Establishment and characterization of a SV40 transformed human fetal gastric epithelial cell line-GES-1]. *Zhonghua zhong liu za zhi*. 1994;16(1):7–10. Chinese.
55. Zhao L, Pan YL, Gang Y, et al. Identification of GAS1 as an Epirubicin Resistance-related Gene in Human Gastric Cancer Cells with a Partially Randomized Small Interfering RNA Library. *J Biol Chem*. 2009;284(39):26273–26285.
56. Griffin J, Singh AK, Senapati D, et al. Size- and distance-dependent nanoparticle surface-energy transfer (NSET) method for selective sensing of hepatitis C virus RNA. *Chemistry*. 2009;15(2):342–351.
57. Hua J, Gross N, Schulze B, et al. In vivo imaging of choroidal angiogenesis using fluorescence-labeled cationic liposomes. *Mol Vis*. 2012;18:1045–1054.
58. Pacardo DB, Neupane B, Rikard SM, et al. A dual wavelength-activatable gold nanorod complex for synergistic cancer treatment. *Nanoscale*. 2015;7(28):12096–12103.
59. Wang J, Zhu G, You M, et al. Assembly of aptamer switch probes and photosensitizer on gold nanorods for targeted photothermal and photodynamic cancer therapy. *ACS Nano*. 2012;6(6):5070–5077.
60. Almeida RD, Manadas BJ, Carvalho AP, Duarte CB. Intracellular signaling mechanisms in photodynamic therapy. *Biochim Biophys Acta*. 2004;1704(2):59–86.
61. Castano AP, Mroz P, Hamblin MR. Photodynamic therapy and anti-tumour immunity. *Nat Rev Cancer*. 2006;6(7):535–545.
62. Vankayala R, Kuo C-L, Sagadevan A, Chen P-H, Chiang C-S, Hwang KC. Morphology dependent photosensitization and formation of singlet oxygen (<sup>1</sup>Δg) by gold and silver nanoparticles and its application in cancer treatment. *J Materials Chemistry B*. 2013;1(35):4379–4387.
63. Huang X, Tian XJ, Yang WL, Ehrenberg B, Chen JY. The conjugates of gold nanorods and chlorin e6 for enhancing the fluorescence detection and photodynamic therapy of cancers. *Phys Chem Chem Phys*. 2013;15(38):15727–15733.
64. Ali MR, Rahman MA, Wu Y, et al. Efficacy, long-term toxicity, and mechanistic studies of gold nanorods photothermal therapy of cancer in xenograft mice. *Proc Natl Acad Sci U S A*. 2017;114(15):E3110–E3118.
65. Kessel D, Reiners JJ Jr. Apoptosis and autophagy after mitochondrial or endoplasmic reticulum photodamage. *Photochem Photobiol*. 2007;83(5):1024–1028.
66. Chiu SM, Oleinick NL. Dissociation of mitochondrial depolarization from cytochrome c release during apoptosis induced by photodynamic therapy. *Br J Cancer*. 2001;84(8):1099–1106.
67. Chiu S, Evans HH, Lam M, Nieminen A, Oleinick NL. Phthalocyanine 4 photodynamic therapy-induced apoptosis of mouse L5178Y-R cells results from a delayed but extensive release of cytochrome c from mitochondria. *Cancer Lett*. 2001;165(1):51–58.
68. Kessel D, Luo Y. Photodynamic therapy: a mitochondrial inducer of apoptosis. *Cell Death Differ*. 1999;6(1):28–35.
69. Bahar E, Kim H, Yoon H. ER stress-mediated signaling: action potential and Ca<sup>2+</sup> as key players. *Int J Mol Sci*. 2016;17(9).
70. Muehlmann LA, Rodrigues MC, Longo JP, et al. Aluminium-phthalocyanine chloride nanoemulsions for anticancer photodynamic therapy: Development and in vitro activity against monolayers and spheroids of human mammary adenocarcinoma MCF-7 cells. *J Nanobiotechnol*. 2015;13(36):1–11.
71. Hong EJ, Choi DG, Shim MS. Targeted and effective photodynamic therapy for cancer using functionalized nanomaterials. *Acta Pharm Sin B*. 2016;6(4):297–307.
72. Bharathiraja S, Moorthy MS, Manivasagan P, Seo H, Lee KD, Oh J. Chlorin e6 conjugated silica nanoparticles for targeted and effective photodynamic therapy. *Photodiagnosis Photodyn Ther*. 2017;19:212–220.
73. Jiang BP, Zhang L, Guo XL, et al. Poly(N-phenylglycine)-based nanoparticles as highly effective and targeted near-infrared photothermal therapy/photodynamic therapeutic agents for malignant melanoma. *Small*. 2017;13(8). Epub 2016 Dec 16.
74. Wang J, You M, Zhu G, et al. Photosensitizer-gold nanorod composite for targeted multimodal therapy. *Small*. 2013;9(21):3678–3684.

## International Journal of Nanomedicine

### Publish your work in this journal

The International Journal of Nanomedicine is an international, peer-reviewed journal focusing on the application of nanotechnology in diagnostics, therapeutics, and drug delivery systems throughout the biomedical field. This journal is indexed on PubMed Central, MedLine, CAS, SciSearch®, Current Contents®/Clinical Medicine,

Submit your manuscript here: <http://www.dovepress.com/international-journal-of-nanomedicine-journal>

Dovepress

Journal Citation Reports/Science Edition, EMBase, Scopus and the Elsevier Bibliographic databases. The manuscript management system is completely online and includes a very quick and fair peer-review system, which is all easy to use. Visit <http://www.dovepress.com/testimonials.php> to read real quotes from published authors.